INTRAMODALITY AND INTERMODALITY REGISTRATION OF THE LIVER

by

Wen-Chi Christina Lee

BS, University of Rochester, 2001

Submitted to the Graduate Faculty of

School of Engineering in partial fulfillment

of the requirements for the degree of

Master of Science

University of Pittsburgh

2003

UNIVERSITY OF PITTSBURGH

SCHOOL OF ENGINEERING

This dissertation was presented

by

Wen-Chi Christina Lee

It was defended on

November 7th, 2003

and approved by

Fernando E. Boada, PhD
Associate Professor, Dept. of Radiology & Bioengineering

George D. Stetten, MD, PhD
Assistant Professor, Dept. of Bioengineering

Brian E. Chapman, PhD
Assistant Professor, Dept. of Radiology & Biomedical Informatics & Bioengineering
Thesis Advisor

ABSTRACT

INTRAMODALITY AND INTERMODALITY REGISTRATION OF THE LIVER

Wen-Chi Christina Lee, M.S.

University of Pittsburgh, 2003

Radiological imaging of the liver is an important medical problem. The ever increasing amount of data acquired when imaging the liver makes integration of information desirable and crucial in building up a comprehensive diagnostic picture of the patient. The foundation of all such image integration is image registration.

Image registration is the process of aligning images so that corresponding features can easily be related, including: (1) landmark-driven methods, (2) surface-based methods, and (3) voxel similarity-based methods.

A challenge with registering the liver is that the liver moves within the abdomen with respiration. Therefore any effective alignment of the liver must first separate the liver from the remainder of the image. With this as a constraint, the goal of this research effort was to determine the feasibility and efficacy of surface-based and voxel similarity-based schemes in registering abdominal CT and MR images with and without contrast.

A multi-scale surface fitting technique was implemented based on the Head and Hat algorithm. Equivalent surfaces from the in vivo images were extracted manually. The hand segmentation approach was validated by ensuring the volume of the liver of each image from the

same patient was consistently within ±7% of one another. The registration transformation was determined by iteratively transforming the hat with respect to the head surface, until the closest fit of the hat onto the head was found.

In addition, registration of in vivo CT and MR images was performed using a multi-resolution mutual information scheme distributed with the ITK Insight software package (National Library of Medicine, Bethesda, MD). As an independent measure of registration accuracy, the mean displacement of automatically selected point landmarks was evaluated. For the multi-resolution mutual information approach, mean misregistrations were in the range of 7.7-8.4mm for CT-CT intramodality registration, 8.2mm for MR-MR intramodality registration, and 14.0-18.9mm for CT-MR intermodality registration. For the Head and Hat surface registration scheme, mean misregistrations were in the range of 9.6-11.1mm for CT-CT intramodality registration, 9.2-12.4mm for MR-MR intramodality registration, and 15.2-19.0mm for MR-CT intermodality registration.

TABLE OF CONTENTS

LIST OF FIGURES

ACKNOWLEDGEMENTS

The completion of this thesis would not have been possible without the help and encouragement of numerous people. I would like to thank my thesis advisor, Dr. Brian Chapman, for his advice and guidance throughout the course of my Master's degree studies at the University of Pittsburgh. His infinite patience in reviewing and editing this thesis manuscript is sincerely appreciated. I am also thankful to Dr. George Stetten and Dr. Fernando Boada for taking the time to serve on my committee, as well as providing me with insightful comments and suggestions.

I also wish to thank the faculties and staffs from the Department of Bioengineering and Department of Radiology for such a unique research and learning environment. Finally, and most importantly, I would like to thank all my friends and family, especially my parents, for their infinite love and support.

1.0 INTRODUCTION

To visualize non-invasively human internal organs in their true form and shape has intrigued mankind for centuries. When Wilhelm Roentgen discovered what he called “a new kind of light” more than a century ago, he never anticipated that medical imaging would make such a vast impact on science, engineering, and medicine. Today, medical imaging has advanced to a stage that was inconceivable 100 years ago, with X-rays, fluoroscopy, ultrasound (US), computed tomography (CT), magnetic resonance imaging (MRI), single photon emission computed tomography (SPECT), and positron emission tomography (PET) scans becoming an integral part of modern healthcare. The introduction of these new technologies has increased the amount of information available to the clinicians, making computational techniques used to assist in the analysis of medical images desirable. The work of this thesis takes steps towards making the integration of useful data obtained from multiple imaging modalities beneficial to the diagnosis of hepatocellular carcinoma (HCC).

1.1 GOALS AND CLINICAL MOTIVATION

Hepatocellular carcinoma (HCC) is the most common intra-abdominal malignancy worldwide with devastating mortality rates. HCC is most common in East Asia and Africa, however, the incidence of HCC is on the rise in the United States and Europe. Patients with clinical presentation of HCC have a five year survival rate of only 5%. HCCs commonly occur in the cirrhotic liver, secondary to liver injury due to hepatitis C virus (HVC), hepatitis B virus (HBV) and alcohol abuse [11]. Early detection is crucial for the treatment of HCC. If detected

early, before the onset of metastasis, HCCs can be successfully cured with liver resection or orthotopic liver transplantation.

Current techniques used to screen HCCs include tri-phasic contrast enhanced CT and contrast enhanced MR, whereas contrast enhanced CT imaging is the standard technique for working up cirrhotic liver, even though contrast enhanced MR has been reported to have improved sensitivity for the detection of HCCs.

A typical CT screening protocol includes high resolution imaging of the chest and abdomen without contrast, with contrast in the hepatic arterial phase, and with contrast in the portal venous phase. Even at a moderate slice of 5mm, the exams can include over 200 images. The large number of images makes clinical review tedious, and observer fatigue can reduce the detection rate of these tumors. We believe, therefore, that computer aided detection (CAD) will have a positive impact on the detection of HCC. For accurate identification of the tumors, the liver images must have accurate geometric correspondence. Accurate and robust registration is crucial in establishing this correspondence.

1.2 THESIS OVERVIEW

i. The goal of this research effort was to evaluate the performance of surface-based and voxel similarity-based registration schemes in intrasubject CT-CT intramodality registration, intrasubject MR-MR intramodality registration, and intrasubject MR-CT intermodality registration.

ii. A multi-scale surface fitting technique was implemented based on the Head and Hat algorithm proposed by Pelizzari and colleagues that included a manual segmentation approach to delineate the corresponding surfaces.

iii. Global registration of in vivo abdominal CT and MR images was performed using a multi-resolution mutual information scheme distributed with the ITK Insight software package (National Library of Medicine, Bethesda, MD).

iv. As an independent measure of registration accuracy, the mean displacement of automatically selected point landmarks was evaluated.

1.3 GUIDE TO REMAINING CHAPTERS

Chapter 2: Background information on liver imaging and the detection of HCC, the state of medical imaging, image segmentation, image registration, methods used for intramodality and intermodality registration.

Chapter 3: Methods used to register liver images are described in detail, including the logic behind hand segmentation, the algorithm used to perform the head-and-hat surface registration and a voxel similarity scheme based a measure known as mutual information, and the algorithm behind the automatic detection of control point pairs used to evaluate the goodness of registration.

Chapter 4: Results obtained from intrasubject CT-CT intramodality registration, intrasubject MR-MR intramodality registration, and intrasubject MR-CT intermodality registration using the surface fitting technique and ITK's MultiResMIRegistration software are presented in this chapter.

Chapter 5: Discussion of registration results and factors contributing to misregistration; conclusion and work to be done in the future to improve liver registration.

2.0 BACKGROUND

2.1 HISTORY OF MEDICAL IMAGING

In 1895, Wilhelm Roentgen, a German physicist working in his laboratory at the University of Wurzburg, made the "great discovery of the invisible ray" as he was making observations of fluorescence using cathode ray tubes [16]. The potential applications of "Roentgen's ray" (subsequently nicknamed X-rays) in medicine and biology were quickly recognized. In a remarkably short time, scientist and physicians began exploiting this exciting new capability to "see into the body" in a painless, nondestructive way.

Nuclear medicine tomographic imaging and ultrasonography were important developments of the 1950's and 1960's. However, not until the 1970's did the field again witness an "epoch-making" development of similar magnitude to that of Roentgen's discovery when the development of X-ray computed tomography (CT) was witnessed [16]. Transaxial scanning, with a highly collimated rotating X-ray source, coupled with computer-based image reconstruction techniques, provides unambiguous discrimination of soft tissue differences, enabling physicians to examine internal structures of the body with a sensitivity and specificity never available to them before.

When computed tomography (CT) and its powerful cross-sectional images of any selected region of the body were introduced in the mid 1970's, there seemed little need for another imaging technique in addition to this excellent tool. It is not surprising that when the magnetic resonance imaging (MR) technique first entered this remarkable arena, its initial modest efforts were regarded with much skepticism. However, developments over the last twenty-five years have prompted MRI to emerge as a powerful diagnostic imaging technique that

has become the method of choice for many applications. Its ability to provide information about the state of health of organs and tissue in addition to details of their shape and appearance offers major advantages over other methods. MRI can detect differences between normal and diseased tissue in images showing exquisite detail [2]. If the discovery of X-rays gave birth to radiology, the invention of computerized tomography has revolutionized radiology. Magnetic resonance imaging is perhaps what has brought us closer to fulfilling the age-old quest of non-invasive visualization.

2.2 MEDICAL IMAGE ANALYSIS AND PROCESSING

The role of medical imaging has expanded beyond the simple visualization and inspection of anatomic structures. It has become a tool for surgical planning and simulation, intra-operative navigation, radiotherapy planning, and tracking the progress of disease [2]. In many cases, multiple images are acquired from subjects at different times, and often with different imaging modalities, leading to an increase in the amount of imaging data that needs to be processed and analyzed.

Processing and analyzing medical images includes a broad topic of areas, such as image enhancement, image compression and storage, image segmentation and matching or registration, and image-based visualization [41]. Automatic interpretation of medical images is a desirable, albeit very difficult long-term goal, since it can potentially increase the speed, accuracy, consistency, and reproducibility of the analysis.

2.3 IMAGE SEGMENTATION

Segmentation plays an important role in medical image processing. It is a fundamental task in image processing, providing the basis for any kind of further high level image analysis, such as image registration. In many cases, the segmentation process often dictates the outcome of the entire analysis, which further reinforces its significance.

Segmentation can be defined as the identification of "meaningful" image components [26]. It delineates structures of interest and discriminates them from the background and each other. This separation, which is generally effortless and swift for the human visual system, can become a considerable challenge in algorithm development.

A wide variety of automatic segmentation algorithms has been proposed. The most commonly used segmentation techniques fall into two broad categories: (1) region segmentation techniques that look for regions satisfying a given homogeneity criterion, and (2) edge-based techniques that look for an edge between regions with different characteristics.

Automatic segmentation algorithms are desirable since they can drastically decrease the labor intensiveness of manual approaches. However, they tend to produce unsatisfactory results and are unreliable, hence, the interactive or semi-automatic methodology is likely to remain dominant in practice for some time to come [2]. Manual methods yield excellent results because human operators not only apply the existing image data information, but also utilize additional model-based knowledge such as anatomical skills as well as complex psychological cognitive abilities with respect to orientation in space.

2.4 IMAGE REGISTRATION

Image registration is the process of aligning images so that corresponding features can easily be related. Since the mid 1980's medical image registration has evolved from being perceived as a rather minor precursor to some medical imaging applications to a significant sub-discipline in itself. Image registration has also become one of the more successful areas of image processing, with fully automated algorithms available in a number of applications [19].

Why has registration become so important? Medical imaging is about establishing shape, structure, size, and spatial relationships of anatomical structures within the patient, together with spatial information about function and any pathology or other abnormality. Establishing the correspondence of spatial information in medical images and equivalent structures in the body is fundamental to medical image interpretation and analysis.

In many clinical scenarios, images from several modalities may be acquired and the diagnostician's task is to mentally combine or "fuse" this information to draw useful clinical conclusions. This generally requires mental compensation for changes in subject position. Image registration aligns the images and so establishes correspondence between different features seen on different modalities, allows monitoring of subtle changes in size or intensity over time or across population, and establishes correspondence between images and physical space in image guided interventions. Registration of an atlas or computer model aids in the delineation of anatomical and pathological structures in medical images and is an important precursor to detailed analysis [16, 19].

It is common for patients to be imaged multiple times, either by repeated imaging with a single modality, or by imaging with different modalities. It is also common for patients to be imaged dynamically, that is, to have sequences of images acquired, often at many frames per

second. The ever increasing amount of image data required makes it more and more desirable to relate one image to another to assist in extracting relevant clinical information [28]. Image registration can help in this task: inter-modality registration enables the combination of complementary information from different modalities, and intra-modality registration enables accurate comparisons between images from the same modality.

International concern about escalating healthcare costs drives development of methods that makes the best possible use of medical imaging and, once again, image registration can help [16, 19]. However, medical image registration does not just enable better use of images, it also opens up new applications for medical images. These include serial imaging to monitor subtle changes due to disease progression or treatment; perfusion or other functional studies when the subject cannot be relied upon to remain in a fixed position during the dynamic acquisition; and image-guided interventions, in which images acquired prior to the intervention are registered with the treatment device, enabling the surgeon or interventionalist to use the pre-intervention images to guide his or her work [1].

2.4.1 General Scheme

Registration is achieved by applying a spatial ***transformation*** to one image set (which we will refer to as the floating/moving/source image) so that it matches the second image set (reference/target image). Most algorithms proceed by iteratively adjusting the transformation so as to maximize some ***similarity measure*** (or minimize a cost function) computed between the transformed floating image and the corresponding reference image. Finding a suitable transformation usually involves the use of an ***optimization*** algorithm. The registration problem

can be further categorized as those that can assume a ***rigid*** transformation, as opposed to those where rigidity cannot be assumed, where ***non-rigid*** transformation is required.

2.4.2 Transformation Models

The transformation that maps the coordinate system of one image onto the coordinate system of the other image can be either global or local. A transformation model is called global when a change in any one of the parameters influences the transformation of the image as a whole. In a local transformation such a change influences only part of the image.

The transformation can be rigid, affine, projective, or curved. These categories indicate the degree of elasticity of the transformation. A transformation is called rigid if the distance between any two points in one image is preserved when these two points are mapped onto the other image. Rigid transformation is limited to translation and rotation. Rigid-body transformation is generally sufficient for intra-subject and intra-modality registration applications for organs that do not experience significant shape change such as the brain [16, 19, 22].

Scaling is added in affine transformations, which causes a straight line in one image to be mapped onto a straight line in the other image preserving parallelism, but without preserving the angles between these lines.

Projective or perspective transformations map any straight line in one image onto a straight line in the other image, but parallelism between these straight lines is in general not preserved. Projective transformations are used to register projection (X-ray) images to 3D tomographic images.

A curved transformation maps a straight line in one image onto a curve in the other image. Transformations that are curved may be used when one of the images has to be deformed to fit the other image, as in matching images from different patients with an atlas [2]. Using curved transformation when fusing functional images with anatomical images or when deformations sustained by the anatomy are not negligible can provide more accurate registration results.

2.4.3 Optimization

Most registration algorithms require some form of optimizer to determine the "best" solution based on maximizing the relevant similarity measure [4, 5]. Popular optimization techniques include general gradient descent methods and Powell's Direction Set Method. Most of these algorithms are based on an iterative approach, in which an initial estimate of the transformation is used to calculate a similarity measure. The optimization algorithm then makes another (hopefully better) estimate of the transformation, evaluates the similarity measure again, and continues until the algorithm converges, at which point no transformation can be found that results in a better value of the similarity measure, to within a preset tolerance. A common stopping criterion for optimization techniques is the maximum number of function evaluations set by the user. Evaluations halt once the value specified has been reached, and not when convergence criteria have been met.

One of the difficulties with optimization algorithms is that they can converge to an incorrect solution called a "local optimum". There are often multiple optima within the parameter space, and registration can fail if the optimization algorithm converges to the wrong optimum. Various manipulations in the registration procedure, such as interpolation and image

subsampling, generally introduce ripples to the similarity function. Some of these optima can be removed from the parameter space by blurring the images prior to registration (via a hierarchical approach to registration). However, even these strategies do not guarantee against trapping in local optima.

2.4.3.1 Gradient Descent Gradient descent is a function optimization method that utilizes the derivative of the function and the idea of steepest descent [32]. The derivative of a function is simply the slope, and given the slope of a function, one can move the function in the negative direction of the slope to reduce its value. Gradient descent is an attractive optimization method in that it is conceptually straightforward and often converges quickly. Its drawbacks include the fact that the derivative of the function must be available, and it often converges to a local minimum rather than a global minimum.

2.4.3.2 Powell's Direction Set Method Powell's direction set method finds the minimum function value in an N-dimensional parameter space by a succession of one-dimensional optimizations [29, 32]. The advantage of this approach is that one-dimensional optimization is a relatively easy problem to solve numerically. Each iteration involves carrying out N one-dimensional optimizations. For 3D rigid body registration, there are six degrees of freedom (three translations and three rotations) giving a six-dimensional parameter space. It is common to start by carrying out the one-dimensional optimizations along directions defined by the axes of the parameter space. For example, the method might start by searching in the lateral translation direction, then the anterior-posterio translation direction, then the cranial-caudal translation direction, then rotations about each of these axes in turn. This example only gives one of the 6!=720 different orders in which the axes can be searched at the first iteration [29]. The choice of

ordering can influence the success of the optimization, and a heuristic approach is often adopted to select the order of the search [16]. The optimization algorithm halts when an iteration fails to improve the similarity measure evaluation by more than some predefined tolerance. The speed of registration can be increased by applying the Powell optimization algorithm at multiple resolutions [39]. The resolution of the data is reduced by blurring and subsampling the images. The algorithm is run at a lower resolution; then when it terminates, it is started again at a higher resolution, using the solution obtained at the lower resolution as the starting estimate. This increases the speed of the algorithm substantially both because the blurred and subsampled images have fewer voxels than the original, making the similarity measure quicker to calculate at each iteration, and also helps avoid local minima.

2.4.4 Similarity Measures

A measure of similarity between images is central to the registration algorithm. It determines the robustness and flexibility of the algorithm [40]. A number of similarity measures have been suggested, generally falling into three categories: (1) landmark-based measures, (2) surface measures, and (2) voxel intensity measures.

2.4.4.1 Landmark Measures Registration can be achieved by identifying unique landmarks, either anatomically defined or fixed externally to the patient, that appear in the two images to be aligned. Relatively simple and well-developed algorithms can then be used to find the transformation that minimizes the average distance between the corresponding imaged landmarks. Many images, such as nuclear medicine images, lack sufficient anatomical detail to identify specific anatomical landmarks [23]. The use of external fiducial markers is not always applicable, and is generally inconvenient and impractical for routine use.

2.4.4.2 Surface Measures Two images can be aligned by minimizing the average distance between corresponding surfaces, identified by preprocessing the images. An alternative is to match surface points in one image to the identified surface in the second image. This particular technique was among the first to be successfully applied in matching nuclear medicine data to other modalities.

The "Head-and-Hat" Algorithm:

The first investigators to apply surface registration to a medical problem were Pelizzari, Chen, and colleagues. The "head-and-hat" algorithm was originally designed for use in brain studies, for registering CT, MR, and PET images of the brain, but has since been adapted for many other applications. Pelizzari et al. made the assumption that given two 3D models of an object, a unique coordinate transformation can be found which, when applied to one of the models, gives the best possible alignment of the two models [24, 31]. The analogy of finding the optimum placement of a custom fitted rigid hat onto a head seems appropriate and is widely accepted. However, for a highly symmetric object such as a sphere or cylinder, clearly a unique transformation could not be found based only on matching the surfaces [1]. Fortunately, such perfect symmetry seems sufficiently lacking in most human organs.

To begin the surface registration process, 3D models of the surface to be matched are produced by outlining contours on the serial slices of each scan. The model taken from the scan covering a large volume of the patient, or from the scan having higher resolution if volume coverage is comparable, takes the role of the "head" in the "head-and-hat" analogy. The "head" model is a stack of disks or "prisms", each of which has cross section determined by one of the contours, with thickness and vertical position appropriate to the slice in which the contour was made [31]. The second or "hat" model is represented as a set of independent points.

A standard algorithm for minimization of a non-linear function of several variables is used to find the geometric transformation that, when applied to the "hat" coordinates, minimizes the residual mean squared distance between "hat" points and "head" surface. The contribution to the residual for each "hat" point is evaluated by finding the intersection of a ray from the transformed "hat" point to the centroid of the "head" model [16, 19, 24].

The Iterative Closest Point Algorithm:

Iterative closet point (ICP) registration algorithm is another surface-based technique that is now widely used. It represents one surface as a set of points and the other as triangular patches. This algorithm proceeds by finding the closest point on the appropriate triangular patch to each of the points in turn. These close points form a set and are registered using the corresponding landmark-based registration algorithm, and the residual error is computed [28]. New closest points are found and the process continues until the residual error drops by a preset value.

2.4.4.3 Voxel Similarity Measures Voxel similarity-based registration algorithm uses intensities in the two images alone without segmenting or delineating corresponding structures. This method uses all or a large proportion of the data in each image, which tends to average out the error caused by noise and random fluctuations of image intensity. If a linear relationship is exists between voxel intensities in the two images, then the correlation coefficient (CC) is a good major of alignment. Basically, CC involves multiplication of corresponding image intensities. One image is moved with respect to the other until the largest value of the CC is found. Similar measures are sum of squared intensity differences (SSD) where alignment is adjusted until the smallest SSD is found, and ratio image uniformity (RIU) where the variance of the ratio is calculated and alignment is adjusted until the smallest variance is found [12, 16, 19, 22, 23].

When voxel intensities do not differ linearly entropy may be used as a measure of alignment. Entropy (disorder), which is calculated directly from the joint probability distribution, increases with increasing misregistration in both the joint probability distribution and visual appearance of images when overlaid with one another [19]. Minimizing the joint entropy (as calculated from the joint intensity histogram) has been proposed as a basis for registration. However, joint entropy alone does not provide robust measure of image alignment. It is possible to find alternative misalignments that result in a much lower joint entropy.

Entropy:

Image registration can be described as maximizing the amount of shared information in the two images or minimizing the amount of information in the combined image, which suggests the measure of information as a registration metric. The most commonly used measure of information in signal and image processing is the Shannon-Wiener entropy measure H, originally developed as part of the communication theory in the 1940's [19, 27].

$$H = -\sum_i p_i \log p_i$$

H is the average information supplied by a set of i symbols whose probabilities are given by $p_1, p_2, p_3, \ldots, p_i$. This formula satisfies the following three conditions:

(1) The functional should be continuous in p_i;

(2) If all p_i equal $1/n$, where n is the number of symbols, then H should be monotonically increasing in n;

(3) If a choice is broken down into a sequence of choices, then the original value of H should be the weighted sum of the constituent H.

Entropy will have a maximum value if all symbols have equal probability of occurring and a minimum value of zero if the probability of one symbol occurring is one and the probability of all the others occurring is zero. Any change in the data that tends to equalize the probabilities of the symbols $p_1, p_2, p_3, \ldots, p_i$ increases the entropy [19]. Blurring the data reduces noise, and so sharpens the histogram and results in reduced entropy.

Joint Entropy:

In image registration we have two images, A and B, to align. We therefore have two symbols at each voxel location for any estimate of the transformation T. Joint entropy measures the amount of information we have in the combined image. If A and B are totally unrelated, then the joint entropy will be the sum of the entropies of the individual images. The more similar or less independent the image are, the lower the joint entropy compared to the sum of the individual entropies [16, 19].

$$H(A,B) \leq H(A) + H(B)$$

$$H(A,B) = -\sum_{a} \sum_{b} p_{TAB}(a,b) \log p_{TAB}(a,b)$$

Joint entropy can be visualized using the joint histogram computed from the two images (A, B). It can be normalized and regarded as the joint probability distribution function (PDF). The number of elements in the PDF is determined by the range of intensity values in the images. As misregistration increases, the brightest regions of the histogram get less bright and the number of dark regions is reduced. In other words, misregistration reduces the highest values in the PDF and increases the number of zeros in the PDF. So when registering images we want to find a transformation that will produce small number of PDF elements with very high probabilities and give us as many zero probability elements in the PDF as possible, which will

minimize joint entropy [16, 19]. Estimations of probability distributions are usually obtained by simple normalization of the joint histogram, although other schemes are also used.

Mutual Information:

Unfortunately, joint entropy suffers from the overlap problem. One solution to this problem is to consider information contributed to the overlapping volume by each image as well as with the joint information. The information contributed by the images is simply the entropy portion of the image that overlaps with the other image volume [27]:

$$H(A) = -\sum_{a} p_{TA}(a) \log p_{TA}(a)$$

$$H(B) = -\sum_{b} p_{TB}(b) \log p_{TB}(b)$$

where p_{TA} and p_{TB} are the marginal probability distributions (i.e. projection of the joint PDF onto the axes corresponding to intensities in images A and B).

Marginal entropies are not constant during the registration process. They are dependent on the transformation T. While the information content of images being registered is constant, the information content of the portion of each image that overlaps with the other image will change with each change in the estimated registration transformation T [16, 19, 27].

Communication theory provides a technique for measuring the joint entropy with respect to the marginal entropies. This technique is based on the concept of mutual information, which in general terms is a measure of how well one image explains the other. It is based on the assumption that the statistical dependence between corresponding voxel intensities is maximal when the images are geometrically aligned (i.e. when joint entropy is minimized while marginal entropies are maximized). Therefore, one seeks a transformation that transforms one image to a

position where the uncertainty of the other image is minimized or where the amount of information one image contains about the other is maximal [27].

Mutual information *I(A,B)* varies more smoothly with misregistration than joint entropy *H(A,B)*.

$$I(A,B) = \sum_{a} \sum_{b} p_{TAB}(a,b) \log(p_{TAB}(a,b) / p_{TA}(a) * p_{TB}(b))$$

To maximize *I(A,B),* there needs to be a balance between marginal entropies and the joint entropy. The joint entropy is minimal when the joint distribution is minimally dispersed (crisp) and this corresponds to registration. Misalignment will introduce new combinations of gray values and decrease probabilities of the correct combination [16, 19, 27].

The conditional probability (p(b|a)) is the probability *B* will take the value *b* given that *A* has the value *a*. Given this definition, conditional entropy is therefore the average of the entropy of *B* for each value of *A*, weighted according to the probability of getting that value of *A* [27].

$$H(B \mid A) = -\sum_{a,b} p_{TAB}(a,b) \log p_T(b \mid a) = H(A,B) - H(A)$$

Using the equation above, the equation for mutual information can be rewritten as:

$$I(A,B) = H(A) - H(B \mid A) = H(B) - H(A \mid B)$$

The conditional entropy term will be small when the image is predictable by the other, but it will also be small if the image itself is predictable.

Mutual Information and Misregistration:

Mutual information-based matching is also prone to misregistation. The mutual information registration function can be ill-defined containing local maxima when images are of low resolution, when images contain little information, when only a small region of overlap is present, or as a result of interpolation methods. The search for maxima in the mutual information

function may not necessarily lead to absolute maxima. For example, if two image volumes overlap for 5% and if the intensity distributions in the volume of overlap happened to be nearly identical, mutual information would be extremely high [16]. However, this would not be the desired solution since the two volumes virtually do not overlap.

2.5 CLINICAL APPLICATION OF REGISTRATION

2.5.1 Liver Anatomy

The liver is a mobile organ that sits within the abdominal cavity, and its position is variable depending on the position of the patient. It has a variety of ligamentous attachments to the diaphragm, and therefore its physical space position is also dependent on the point in the respiratory cycle. The liver has a dual blood supply: normal parenchyma is primarily fed by the portal venous system, tumors in their early stages of progression also primarily rely on the portal venous system for blood supply; as tumors develop, their blood supply switches from portal to hepatic.

2.5.2 HCC

Hepatocellular carcinoma (HCC) is the most common primary cancer of the liver worldwide, particularly in Asia. It is an infrequent cancer in developed countries, however, its incidence has been on the rise in the United States, and has almost doubled over the past 20 years [11]. There are three main risks for HCC: infection with hepatitis C virus (HCV), infection with hepatitis B virus (HBV), and alcoholic cirrhosis. HCC is a devastating cancer, with an overall 5-year survival rate below 5%. The high mortality rate is due in part to late clinical presentation of

the disease. Therefore, early detection of HCC is important because the disease is curable with liver surgical resection or orthotopic liver transplantation before the onset of metastasis.

2.5.3 Early Detection of HCC and the Need for Image Registration

The detection of small HCC (less than 20mm) using standard clinical imaging protocols is poor. Early radiological detection is problematic. Peterson et al. at the University of Pittsburgh studied a cohort of 430 liver transplant patients and found that pre-transplant CT prospectively detected only 37% of the HCC nodules detected by pathology after transplantation. The visualization and prompt detection of dysplastic nodules and small HCC's is essential. Early staging and accurate surveillance of patients at risk is important for timely interventions or therapeutic decisions. It is believed that computer aided detection (CAD) can have a positive impact on the detection of early stage HCC. Accurate and robust registration is crucial for a functional CAD system.

3.0 MATERIALS AND METHODS

3.1 CT AND MR DATA

The retrospective data used in this project were obtained from patients (mostly liver transplantation candidates) at the University of Pittsburgh Medical Center who were screened for Hepatocellular Carcinoma (HCC) in 2001. Most of the livers were cirrhotic and infected with the hepatitis C virus (HCV). A CT protocol consisted of pre-contrast and post-contrast biphasic (hepatic phase & portal phase) imaging of the liver was performed. The CT images were reconstructed and stored in the radiology PACS system with 5mm slice thickness and in-plane resolution of 0.7mm - 0.9mm. An MR protocol consisted of multiple T2 weighted, and pre-T1 and post-contrast T1 images of the abdomen was also performed on a number of patients to establish correlation with complementary CT scans. The MR images had slice thicknesses of 10mm and in-plane resolution of 1.1mm - 1.5mm. While contrast enhanced MR has been reported to have improved sensitivity for the detection of HCCs, the low cost, rapid imaging time and high spatial and temporal resolution achievable with multi-slice helical CT makes tri-phasic contrast enhanced CT the standard technique for working up cirrhotic livers [13, 21]. Figure 1 shows an example of tri-phasic CT and contrast enhanced hepatic phase MR image set.

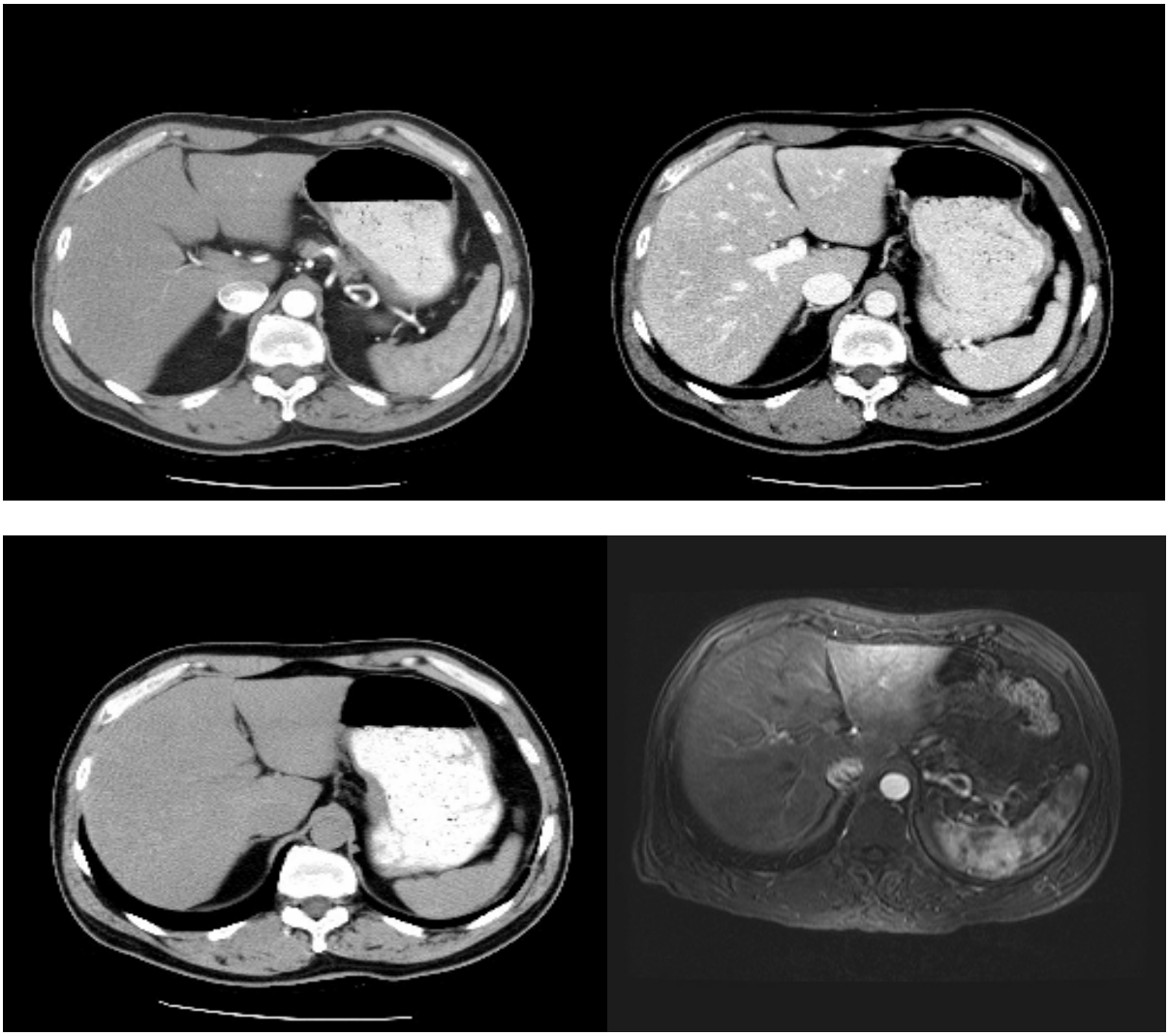

Figure 1: Example CT/MR image set: (upper left) hepatic phase, (upper right) portal phase, (lower left): pre-contrast, (lower right) MR hepatic phase.

3.2 PRE-PROCESSING

DICOM images were retrieved from the radiology PACS system, identified and marked as pre-contrast and contrast enhanced (i.e. hepatic, portal, etc.). Using the hepatic phase volume as the target, the pre and portal volumes were cut to match as nearly as possible the coverage of the hepatic phase volume.

3.3 LIVER SEGMENTATION

Surface-based registration algorithms require identification and delineation of corresponding surfaces in the two images to be aligned. Automatic liver segmentation is difficult, mainly due to the similarity in intensity values between the liver and many contiguous organs.

Because the focus of this project was on image registration, we did not seek to use a fully automated segmentation algorithm. After attempts to automate extraction of the liver from CT images using level sets, histogram methods similar to Gao [15] and Soler [38] and morphology approaches similar to Kaneko et al.[20] drew inclusive results, we resorted to an interactive, manual approach where outlines of the liver were drawn, reviewed and edited.

In preparation for surface registration, liver surfaces from each of the in vivo images were delineated by outlining the liver by hand in a slice by slice manner. The hand segmentation consisted of the user placing control points around the border of the liver and using cubic splines to interpolate a complete border (as shown in Figure 2). The software used for manual segmentation was implemented in IDL (Research Systems, Boulder, CO). Major hepatic vessels such as hepatic artery proper and hepatic portal vein were included in the outlines whereas the aorta and inferior vena cava were excluded.

Masks were constructed from the control points and the volume of liver or the number of voxels within each mask was computed as a measure of the consistency of these outlines. The volume percentage error between a chosen reference image (usually the hepatic phase image) and any image of the same patient from the same study was calculated and kept under 7%. Liver outlines that did not satisfy this requirement were reviewed and edited. An abdominal radiologist was consulted to ensure accurate identification and delineation of the liver.

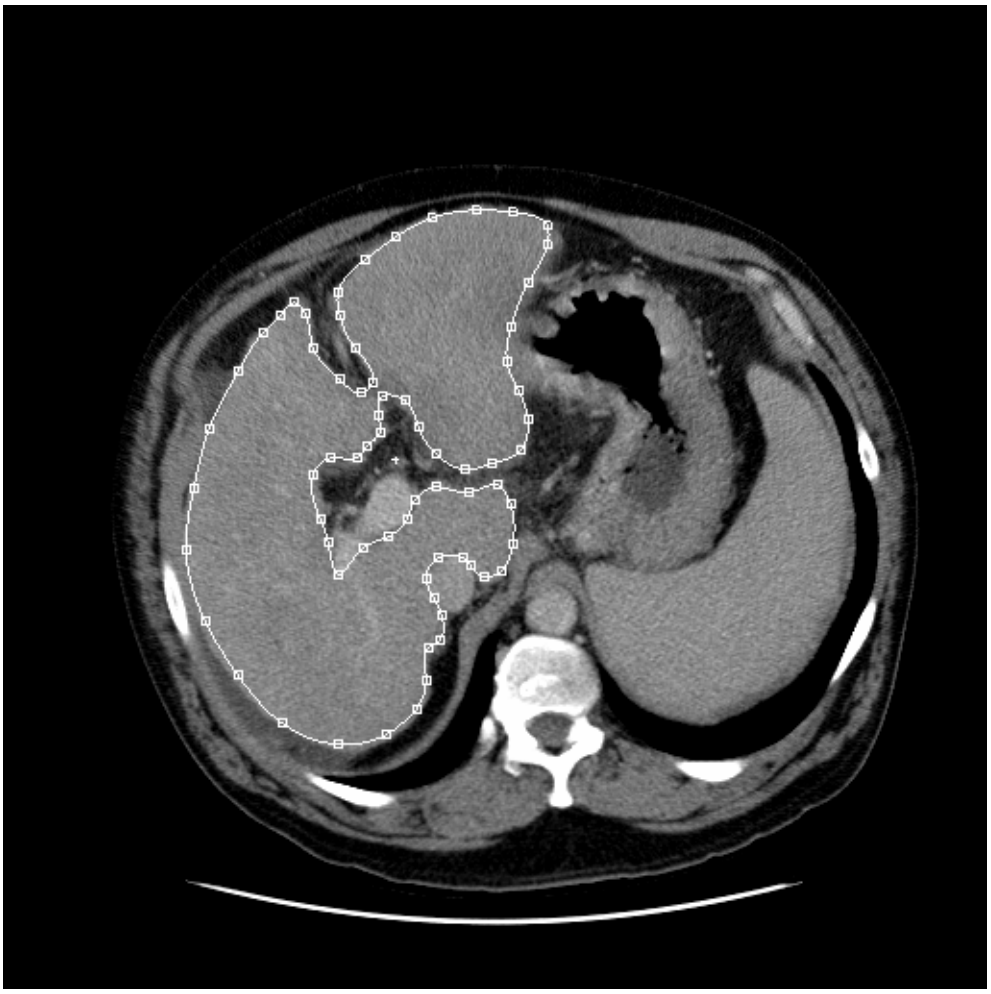

Figure 2: Hand segmentation software with user-placed control points around the border of the liver.

26 CT cases and 13 MR cases were processed and outlined, from which 18 CT cases and 5 MR cases with satisfactory volume percentage errors were selected for registration. A number of CT and MR cases had notable liver volume differences, typically associated with large discrepancy in voxel size of pre-contrast and post-contrast images. The CT images were all of high resolution, whereas only one MR case contained high resolution images.

3.4 HEAD AND HAT SURFACE REGISTRATION

Pelizzari and colleagues proposed a surface fitting technique for intermodality registration of images of the head that became known as the "head-and-hat" algorithm [18, 24, 31]. A multi-resolution version of this surface-based registration technique was implemented in C++ and Python (ActiveState Corp., Melbourne, Australia) to register images of the liver. The multi-resolution behavior was achieved by subsampling the surfaces by decreasingly smaller amounts. The head and hat error measure was implemented in C++ for speed, while the parameter optimization was done in Python using the implementation of Powell's method in the SciPy package.

Two equivalent surfaces were identified in the images to be aligned using the manual segmentation approach described in the previous section. The first, from the pre-contrast CT image in CT-CT intramodality registration, contrast enhanced MR hepatic phase image in MR-MR intramodality registration and MR-CT intermodality registration, was represented as a list of unconnected 3D points and denoted as the "head." The second surface, the "hat," was an equivalent list of unconnected 3D points from the contrast enhanced portal and hepatic phase CT images in CT-CT intramodality registration, each of the pre-contrast and post-contrast MR images in MR-MR intramodality registration and pre-contrast CT, contrast enhanced hepatic and portal phase CT images in MR-CT intermodality registration. Figure 3 shows the fitting of the hat onto the head. The top figure shows aligned contours of a sample intrasubject CT-CT intramodality registration in progress. The bottom figure shows misaligned contours of sample MR and CT volumes.

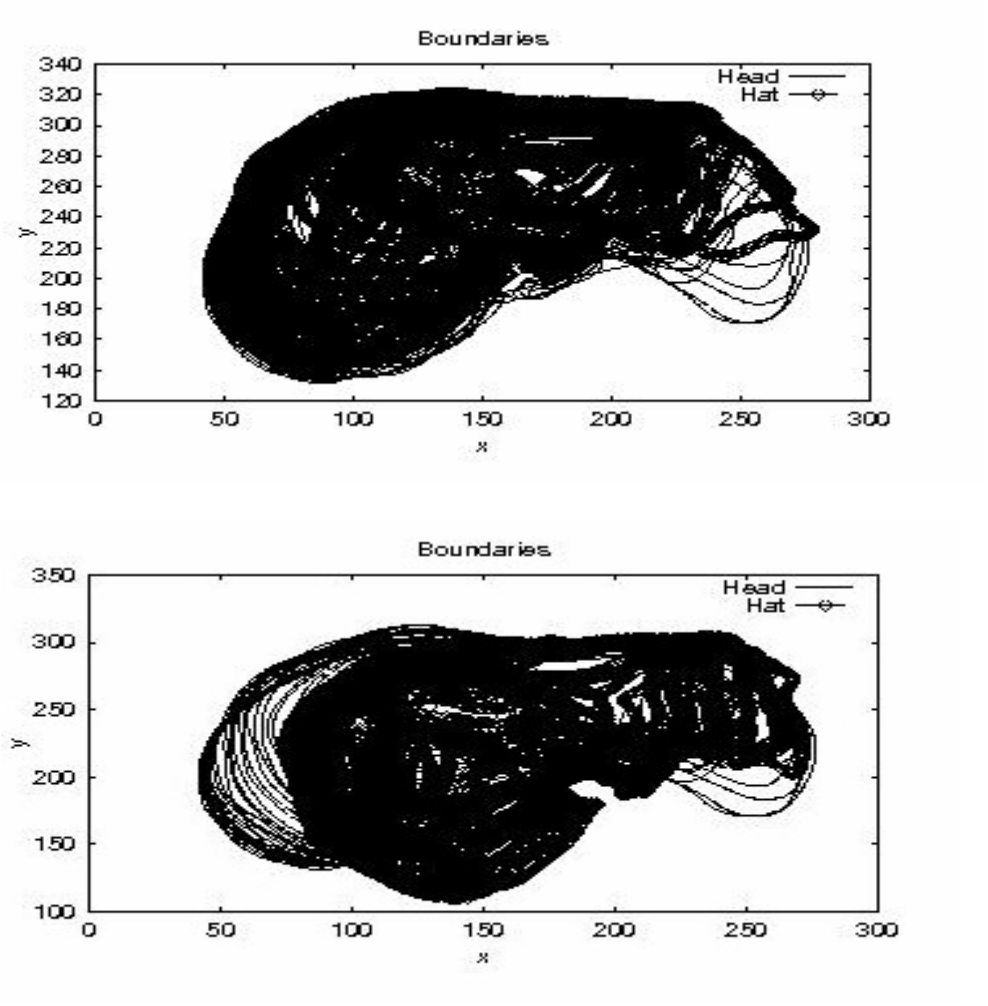

Figure 3: Surface fitting of the hat onto the head: (top) aligned contours vs. (bottom) misaligned contours.

The registration transformation was determined by iteratively transforming the rigid hat surface with respect to the head surface, until the closest fit of the hat onto the head was found. The measure of closeness of fit used was the square of the distance between a point on the hat and the nearest point on the head, in the direction of the centroid of the head. The Powell optimization algorithm performed a succession of one dimensional optimizations, finding in turn the best solution along each of the six degrees of freedom.

Since quantitative validation was difficult to implement because the ground truth was not known, we took a self-validation approach to determine the accuracy of the surface fitting program by transforming the secondary volume in an otherwise registered image pair to simulate a pair of misaligned volumes. The goal of registration was then to overcome the user-introduced transformation by applying an exactly opposite transformation to the secondary volume. Comparing the known transformation with the solution of the registration allowed us to determine the accuracy of our registration software.

Armed with the lessons learned from the validation approach described above, we carried out intrasubject CT-CT intramodality registration, intrasubject MR-MR intramodality registration and intrasubject MR-CT intermodality registration using a deterministic multi-resolution approach that subsampled each surface by factors of 128, 64, 32, 16, 8, and also using a stochastic multi-resolution approach that subsampled surfaces by 128, 64 and 32 with 17, 14 and 11 randomly chosen starting points for parameter optimization. A selected number of cases were also subsampled at 128, 64, 32, 16, 8 with 17, 14, 11, 8, 5 starting points. Each contrast enhanced CT image was registered to the pre-contrast CT image, whereas each MR image was registered to the contrast enhanced hepatic phase MR image. For MR-CT intermodality registration, each CT image (pre-contrast or post-contrast) was registered to the MR contrast enhanced hepatic phase image. The MR target surface and each of the moving CT surfaces were subsampled by different factors to ensure that the number of surface points was consistent. Also, the final transformation parameters found by the surface fitting program was modified to compensate for the difference in resolution and field of view in the MR target and CT moving images.

The overall registration accuracy of the surface fitting technique was measured using the mean displacement of automatically selected landmarks proposed by Wang et al [43]. The landmarks were selected based on the similarity in intensity values between a given set images. 20 landmarks were selected from the target image and the moving image, and based on visual inspection and the mean displacement between corresponding landmarks, we were able to determine the nature of misregistration both qualitatively and quantitatively.

3.5 MUTUAL INFORMATION

Mutual information is a measure from the field of information theory of how much information one random variable tells about another. It was introduced as a measure for matching medical images in 1995 by both Viola and Wells and by Collignon [16, 19, 27]. For two images, mutual information is computed from the joint probability distribution of the images' intensity or gray-values. When two images are aligned, corresponding areas overlap, and the resulting joint histogram or probability distribution is "peaky" resulting in a high mutual information value. When the images are misregistered, non-corresponding areas also overlap, resulting in additional gray value combinations in the joint histogram, causing the distribution to disperse and resulting in a low mutual information value [37]. This approach to registration is accepted by many as one of the most accurate and robust registration measures.

3.5.1 ITK

ITK is an abbreviation for the National Library of Medicine Insight Segmentation and Registration Toolkit. ITK is an open-source software system for performing segmentation and

registration of data in two, three and more dimensions, with primary focus on medical applications. The toolkit is implemented using templated C++. It is organized around an object-oriented data flow architecture. Data is presented using data objects (e.g. images). These data objects are processed by process objects (filters). Data objects and process objects are connected together into pipelines. Pipelines can process data in pieces according to a user-specified memory-limit set on the pipeline.

ITK was developed by six principal organizations: three academic (University of North Carolina at Chapel Hill, University of Utah and University of Pennsylvania) and three commercial (GE Research & Development, Kitware and Insightful). Several other small team members and individual users also contribute actively.

ITK has been developed to support the Visible Human Project and to be a repository of fundamental algorithms for image segmentation and registration, saving the medical image community from reinventing the wheel over and over again. The open-source nature of ITK allows developers around the world to freely contribute to the software's further extension and development.

ITK comes in the form of a set of libraries. Pre-compiled version of the libraries are not provided, as a source code archive needs to be downloaded form the ITK website, configured and compiled. With ITK being in a state of relative infancy and without any substantial documentation, getting comfortable with the APT and the ITK programming style was a very challenging task.

3.5.2 Image Registration Using ITK

The registration framework in ITK is modular. Thus, when composing a registration method, each component is relatively independent of the others. Registration methods in ITK are implemented by combining basic components, allowing for great flexibility. When creating a registration filter, the following components are used as defined in ITK:

Fixed image: this is the image onto which we map the moving image.

Moving image: this is the image that will be transformed into the coordinate system of the fixed image.

Transform: a mapping that associates a point in the fixed image space with a point in the moving image space.

Interpolator: a technique used to interpolate intensity values when images are r esampled through the transformed.

Metric: a measure of how well the fixed image matches the moving image after transformation.

Optimizer: a method used to find the transformation parameters that optimize the metric. The most critical components are the metric and the optimizer.

The registration process begins by first applying the initial offset transformation. This initial transform is applied once, after which the registration method takes over to further refine the image alignment. The voxels in the moving image are mapped onto the fixed image using the selected registration transform (rigid transform). As the voxel values are mapped to the fixed image their spatial position will generally be mapped to non-grid positions. The interpolator helps determine what the voxel intensity should be on the grid. The metric (i.e. mutual

information) evaluates how well features in the two images match each other. This is done by comparing the fixed image with the transformed moving image. The role of the optimizer is to keep changing the parameters of the registration transform, searching for a combination that gives the best value of the metric. Thus, the execution of the registration method is ultimately driven by the optimizer.

Recent published works for registration indicate that mutual information-based methods work very well, especially when combined with multi-resolution calculations [27, 37]. To save processing time, the images to be registered may be downsampled to a lower resolution before the registration procedure begins. Registration is performed on the downsampled images for a number of iterations before it continues on the full-resolution images. When registration is complete on one level, it steps up to the next level and the images are registered again, and so on, until the full-resolution images are registered. This increases the performance considerably compared to working with the full-resolution images the entire time.

3.5.3 ITK's MultiResMIRegistration Software

ITK's MultiResMIRegistration software reads in two 3D raw image volumes: the fixed (target) volume and the moving (source) volume. The application then iteratively estimates the rigid transform that will align the moving onto the fixed volume and terminates after completing a user-defined number of iterations. The estimated rigid transform is applied to the moving/source image. Each 2D slice from the fixed, moving and registered image volume is written out as PGM files, facilitating viewing with simple 2D image viewers. The application makes use of the ITK registration framework and ITK multi-resolution framework. The part of the registration framework used by this application are the itk::

QuaternionRigidRegistrationTransform, the itk::LinearInterpolateImageFunction, the itk:: MutualInformationImageToImageMetric and the itk:: GradientDescentOptimizer. Performing image registration using a multi-resolution strategy has been widely shown to improve speed, accuracy and robustness. The ITK multi-resolution registration framework is a generic framework for defining a multi-resolution registration scheme.

The application takes one argument: the name of a parameter file. A valid parameter files contains filename, endian-ness, size, voxel spacing of the raw 3D fixed (target) and moving (source) volumes; axes permutation order; number of multi-resolution levels to be used; starting level shrink factor for the fixed and moving volumes; the number of iterations to be performed at each resolution level; the learning rate at each resolution level; the scale applied to the translation parameters during optimization; and the output directory where the PGM files are to be written to. Both the fixed and moving volumes are assumed to be in binary (signed short) format.

3.5.4 Validating ITK's MultiResMIRegistration Software

In order to evaluate the performance of ITK's MultiResMIRegistration software, a number of digital phantoms (image size=256x256x40, object size=84x84x18, voxel spacing=1mmx1mmx1mm) were created and registered with its identical counterparts subjected to various known amounts of translations and rotations (as shown in figure 4).

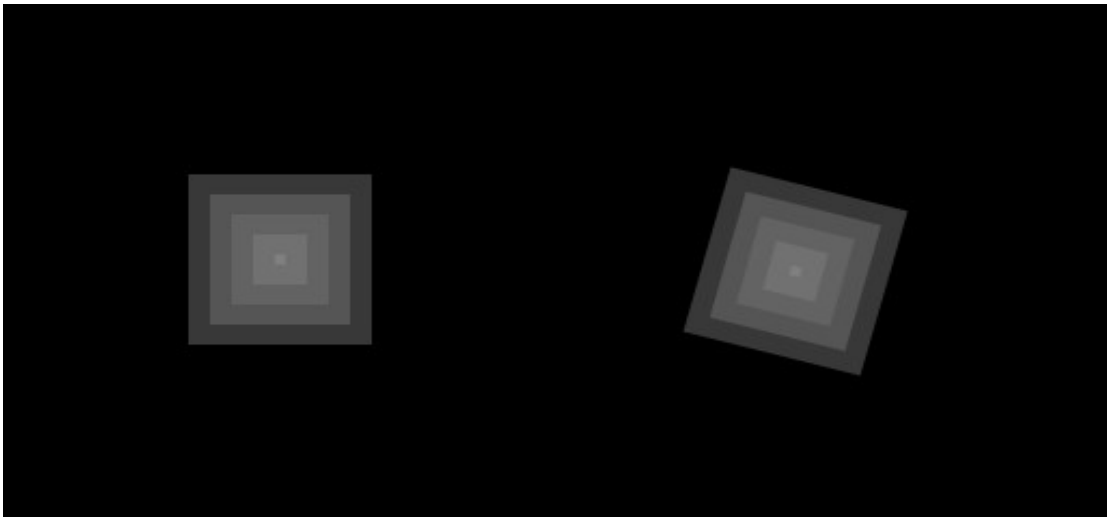

Figure 4: Example digital phantom set.

After extensive correspondence with the ITK developers and lengthy sleepless sessions of trial and error, a set of heuristics for fine tuning the parameters was used to register the phantoms. The one parameter that had the most impact on the "goodness" of registration was the translation scale. The translation scale addresses the difference in scale between the parameters that represent rotation (ranging from 0 to 1 in radians) and the parameters that represent translation (ranging from 0 to the size of the image in mm). The heuristic is to set the translation scale to the maximum dimension in mm. It was found that the MultiResMiRegistration software was unable to recover rotations greater than 18 degrees, and the performance of the program began to decline when the complexity of the transformation grew (four degrees of freedom).

Creation of 3D binary masks, one corresponding to the primary volume and the other to the secondary volume, preceded registration. The masks distinguished image voxels from the background & the surrounding organs & isolated the organ of interest (i.e. the liver).

Each of the CT or MR masked images was registered with a self-derived image subjected to the following transformations using the parameters determined from previous studies on the

phantoms: (1) z-rotation in 15 degrees, (2) x, y, z translations in 15, 10, 5 pixels, respectively, and (3) z-rotation in 15 degrees in addition to shifts in x, y, z of 15, 10, 5 pixels.

For intrasubject CT-CT intramodality registration, the hepatic phase and portal phase images were registered with the pre-contrast image. For intrasubject MR-MR intramodality registration, each MR image, non-contrast enhanced or contrast enhanced, was registered with the contrast enhanced hepatic phase image. For intrasubject MR-CT intermodality registration, each CT image was registered to the contrast enhanced hepatic phase MR image. Initially, each MR image was registered to the hepatic phase CT image but yielded horrendous results. The desired transformation (3 translations and 3 rotations) were computed from the final parameters, overall transform matrix, and overall transform offset outputted by ITK's application. Landmarks or control points were selected from the PGM files for the registered and fixed image volumes to measure the accuracy of the registration scheme.

3.6 MEASURING REGISTRATION ACCURACY

A very important consideration in registration work is the validation of the methods. The variety of parameters used to express "goodness" of registration has led to some confusion in their interpretation [28]. Direct proof of the validity of registration techniques is not easy, and extensive validation is quite demanding in terms of time and effort.

In validating a registration method one needs to demonstrate that the technique is accurate and precise, but also robust (i.e. provides consistent results independent of the starting conditions) and reliable (i.e. adaptable to different data sets).

Because the set of features that can be identified across the different CT phase images is scarce, validation techniques based on the identification of corresponding anatomical landmarks is difficult [18, 37]. As a result, we have resorted to a technique developed by Wang et al. [43] that automatically identifies corresponding landmarks based on image gradients. Most of the control points selected coincided with edges, edge corners and contour ridges. We assessed the accuracy of each image registration algorithm by measuring the mean displacement between these corresponding landmarks. Figure 5 displays a control point pair found using the automatic control point detection algorithm. The points seem to correspond to the same anatomical feature in the two images. The mean displacement between the points is roughly 4.3.

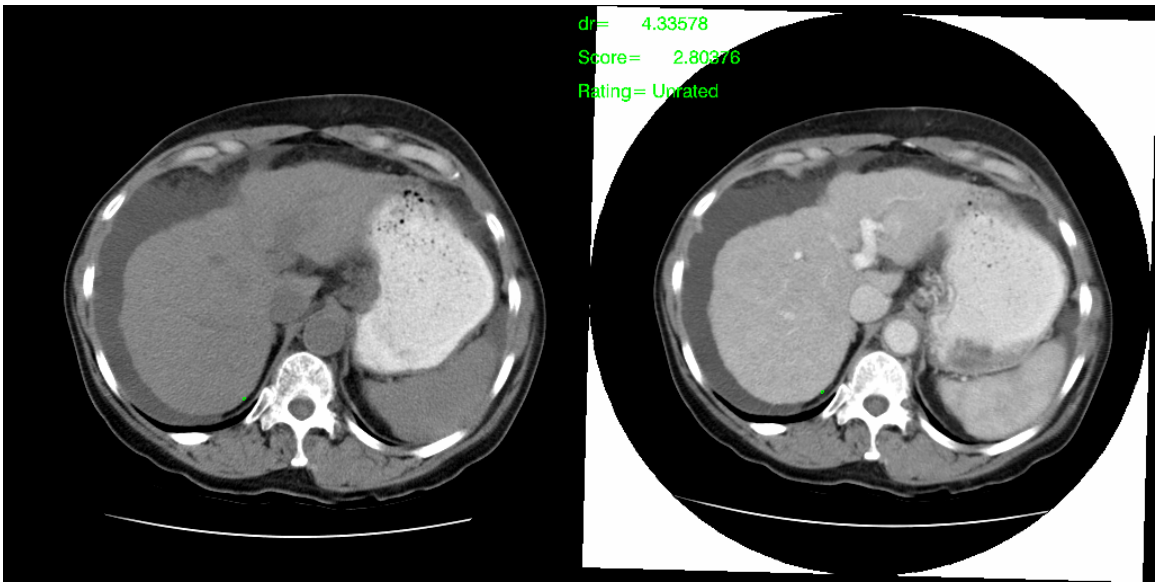

Figure 5: Control point pair (in green) found using the automatic control point detection algorithm. The mean displacement between these points is the mean misregistration value.

3.6.1 Automatic Control Point Detection

The automatic control point detection algorithm (ACPD) was implemented in IDL (Research Systems, Boulder, CO) as follows. The gradient *Gt* for the reference/target image and

the source/moving image were computed and denoted as *IGtr* & *IGts*. For each point in *IGtr*, the average gradient *avgGr* was computed [43]. An initial point list for the reference image was created containing points with *Gtr* > *avgGr*. The list was sorted in decreasing order of *avgGr*, and for each current point *p*, all points appearing further on in the list which belong to the neighborhood *Np* (search window) of *p* were deleted. The result was a list of control points in the reference image, whose neighborhoods did not overlap.

For each point *p* in the list, all corresponding candidate points *p'* in *IGts* were found, and for each corresponding pair, the correlation between the local windows centered on *p* and *p'* was calculated individually. The point in the source/moving image around *p* with optimal correlation value, either from the original window or rotated window, was used to determine the best matched point *p'* and was added to the matched point list 2.

4.0 RESULTS

4.1 HEAD AND HAT SURFACE REGISTRATION

4.1.1 Self-Validation Results

A self-validation approach was used to determine the accuracy of the "head-and-hat" surface registration program by applying a known transformation to an image to simulate a pair of misaligned volumes. Small randomly induced x-, y-, z-translations between -15mm and 15mm were used.

Each CT surface was subsampled by a factor of 64. Ten out of 48 surfaces (21%) that were registered found reverse transformations that were many times greater than the induced translations (i.e. the optimizer converged to the wrong optimum in a bumpy parameter search space and led to inaccurate transformation parameters). As an attempt to minimize this divergence, the surfaces were registered using multiple (10, 15, 20) starting points. With 10 starting points, 6 out of 48 cases diverged (12.5%). With 15 starting points, 4 out of 48 cases diverged (8.3%). With 20 starting points, only 2 out of 48 cases showed divergence (4.2%). From the trend observed (shown in figure 6a), we can conclude that the stochastic surface fitting approach based on a "multi-start" optimization scheme performs better when multiple optima exist, and when subsampled by 64, 15 or more starting points are needed to suppress the tendency of the optimizer to diverge.

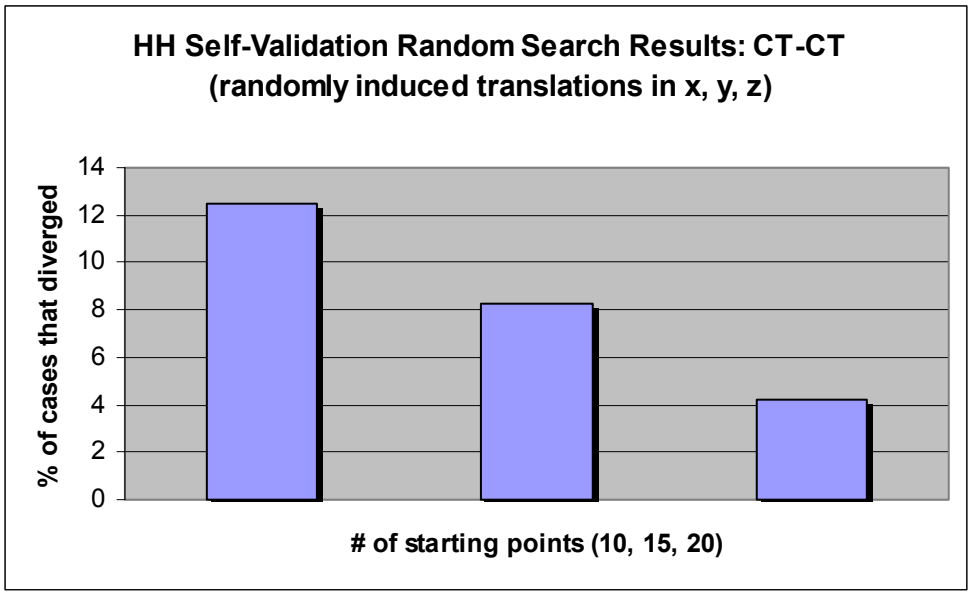

Figure 6a: Self-validation results for the Head & Hat based on a "multi-start" optimization scheme for ***CT-CT validation using randomly induced x, y, z translations***. Note the correspondence between the percentage of cases that diverged and the number of starting points used.

The same validation tests were performed on misaligned image pairs to generate randomly induced z-rotation between -0.3 and 0.3 radians, in addition to the induced shifts described above. The surfaces were subsampled by 64, with 5, 10, 15 and 20 randomly selected starting points. With only 5 starting points, 23 our 54 cases diverged (42.6%). With 10 starting points, 17 out of 54 cases diverged (31.5%). With 15 starting points, 8 out of 54 cases diverged (14.8%). With 20 starting points, 4 out of 54 cases diverged (7.4%). The results are shown in figure 6b. Therefore, it is evident that more "multi-start" points are required to suppress divergence as the complexity of the transformation grows.

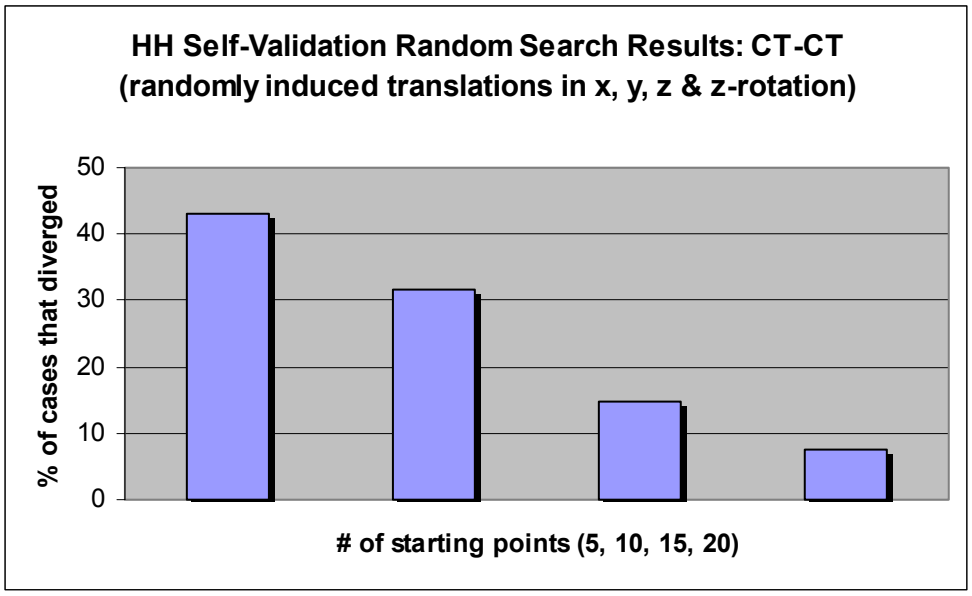

Figure 6b: Self-validation results for the Head & Hat based on a "multi-start" optimization scheme for ***CT-CT validation using randomly induced x, y, z translations plus z-rotation***. Note the drop in the number of cases that diverged and the number of starting points used.

Each MR image was also subjected to the same validation tests. Because the MR data had lower resolutions than the CT data, they were subsampled by a lower amount than the CT data. When the MR data were subsampled by a factor of 16, mean misregistration and percentage/rate of divergence for the MR data sets were significantly larger than that for the CT data. With 5 starting points, 13 out of 30 cases showed divergence (43.3%), with 10 starting points, 12 out of 30 cases diverged (40%), with 15 starting points, 9 out of 30 cases diverged (30%), and with 20 starting points, 6 out of 30 cases diverged (20%). The results are shown in figure 6c. Therefore, the subsampling rate and the number of starting points play an important role in the performance of stochastic surface fitting.

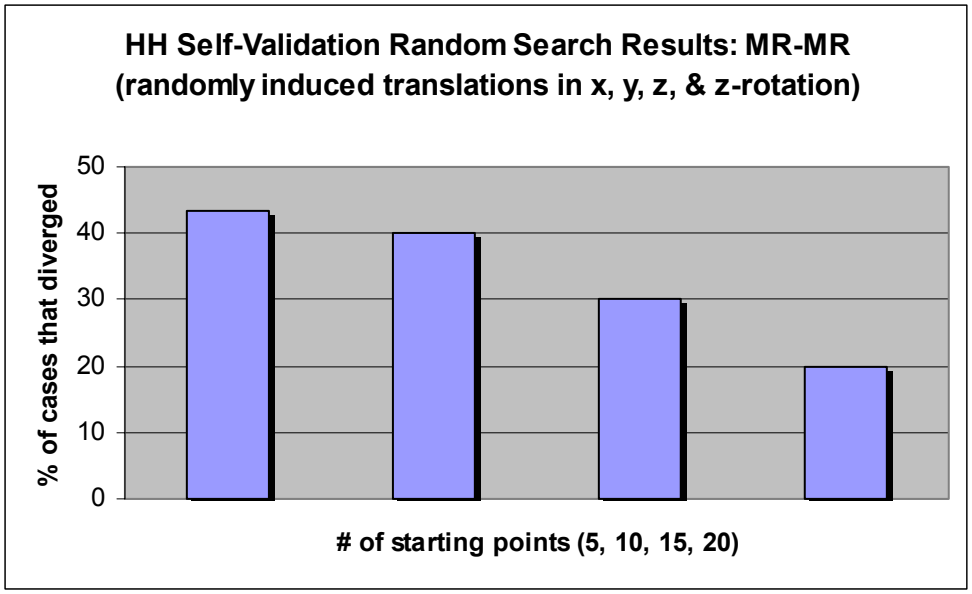

Figure 6c: Self-validation results for the Head & Hat based on a "multi-start" optimization scheme for ***MR-MR validation using randomly induced x, y, z translations plus z-rotation***.

The tendency of the optimizer to converge to the wrong optimum in an ill-behaved parameter space has been observed in the self-validation study. Our solution to the problem of multiple optima was to start the optimization algorithm with multiple starting estimates which result in multiple solutions, and choose the solution with the best value of the similarity measure. This sort of approach, called "multi-start" optimization has been shown to be effective for surface matching algorithms. However, even this "multi-start" strategy could not completely solve the problem of divergence

4.1.2 Results for Intrasubject CT-CT Intramodality Registration

For intrasubject CT-CT intramodality registration, with the pre-contrast CT image as the target and the contrast enhanced hepatic phase image as the source, the mean displacements between the selected landmarks or control points were 10.3mm and 11.1mm for the stochastic approach with 20 initial random starting points. For contrast enhanced portal image as the moving image, the mean displacements by subject were 10.4mm and 9.6mm for the stochastic approach. Figures 7a and 7b are plots of the mean in-plane (dxy) and through-plane (dz) displacements for the deterministic approach and the stochastic approach. The two different schemes produced similar in-plane and through-plane displacement errors for intrasubject CT-CT intramodality registration.

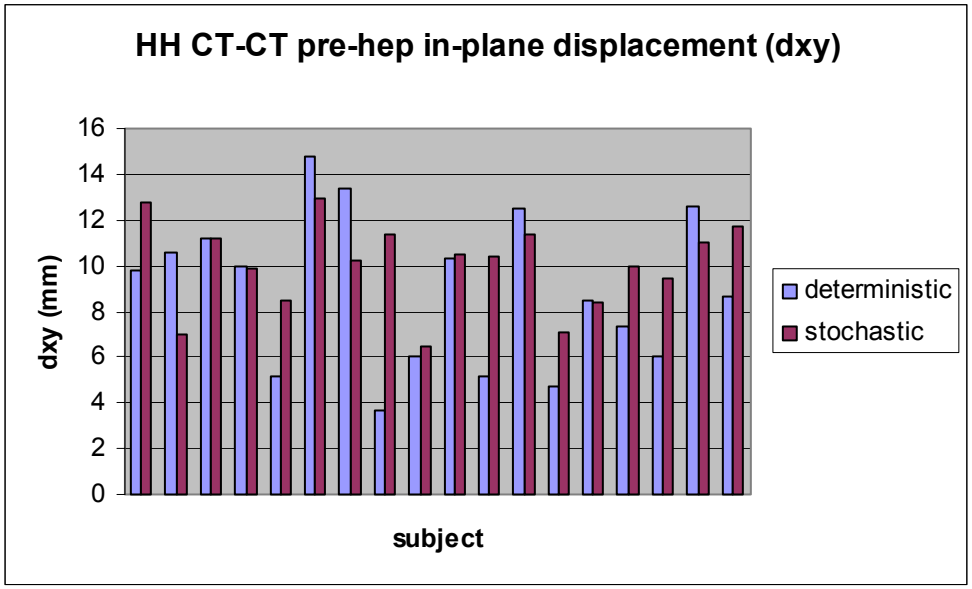

Figure 7a: Plot of in-plane displacement error (dxy) by subject. The "multi-start" (stochastic) optimization scheme failed to show superiority over the deterministic approach in intrasubject CT-CT intramodality registration.

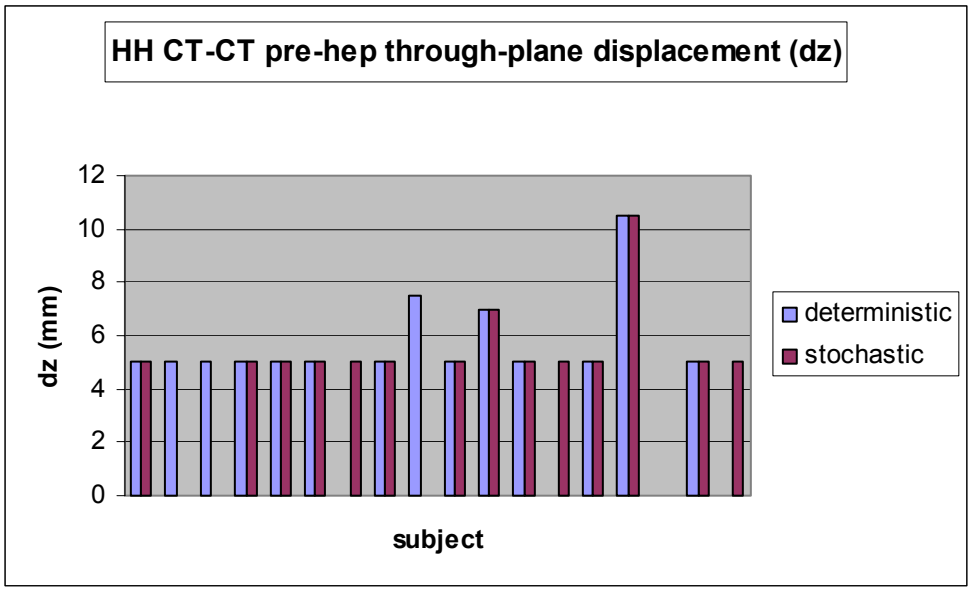

Figure 7b: Plot of through-plane displacement error (dz) by subject. Mean displacements of zero are not plotted.

4.1.3 Results for Intrasubject MR-MR Intramodality Registration and Intrasubject MR-CT Intermodality Registration

For intrasubject MR-MR intramodality registration, the mean displacements by subject were 9.2mm for the deterministic approach and 12.4mm for the stochastic approach. A breakdown of displacement errors (in-plane and through-plane components) is shown in figure 8a and 8b.

For intrasubject MR-CT intermodality registration, with the contrast enhanced MR hepatic phase image as the target and the CT contrast enhanced hepatic phase image as the source, mean displacements between the selected landmarks were 17.2mm and 19mm for the stochastic approach. Plots of the in-plane and through-plane displacement errors are shown in figures 9a and 9b. With the contrast enhanced portal phase CT image as the moving image, the

mean displacements by subject were 15.2mm and 16.4mm for the stochastic approach. With the pre-contrast CT image as the moving image, the mean displacements were 17.9mm and 17.7mm for the stochastic approach. Surprisingly, the deterministic approach performed better than the stochastic approach. As a general observation, the degree of misregistration was significantly larger in MR-CT intermodality registration.

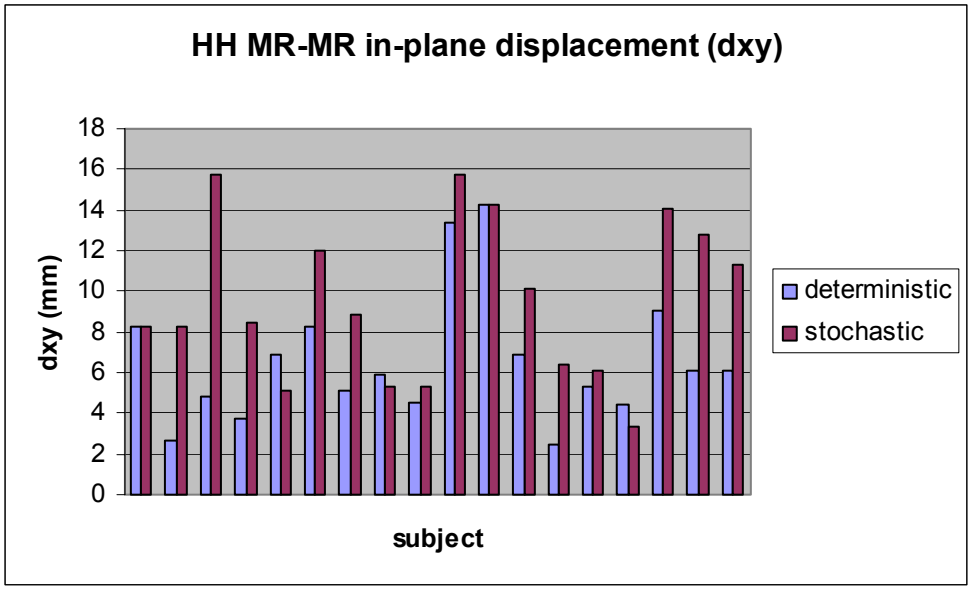

Figure 8a: Plot of in-plane displacement error (dxy) for intrasubject MR-MR intramodality registration. Note the "multi-start" (stochastic) scheme yielded greater in-plane displacements than the deterministic approach.

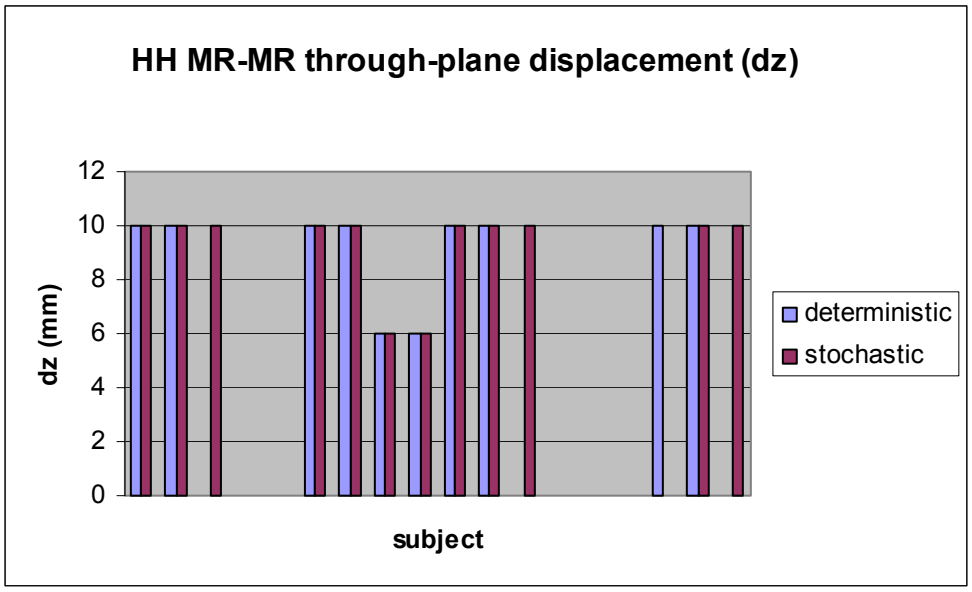

Figure 8b: Plot of through-plane displacement error (dz) for MR-MR registration. Note that mean displacements of zero are not plotted.

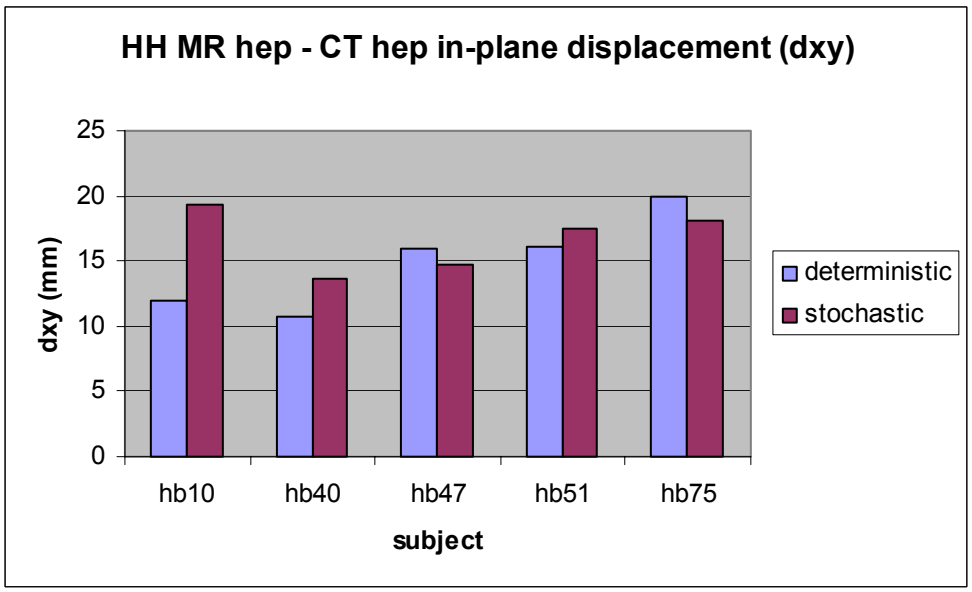

Figure 9a: Plot of in-plane displacement error (dxy) for sample intrasubject MR-CT intermodality registration by subject. The two optimization schemes produced similar results.

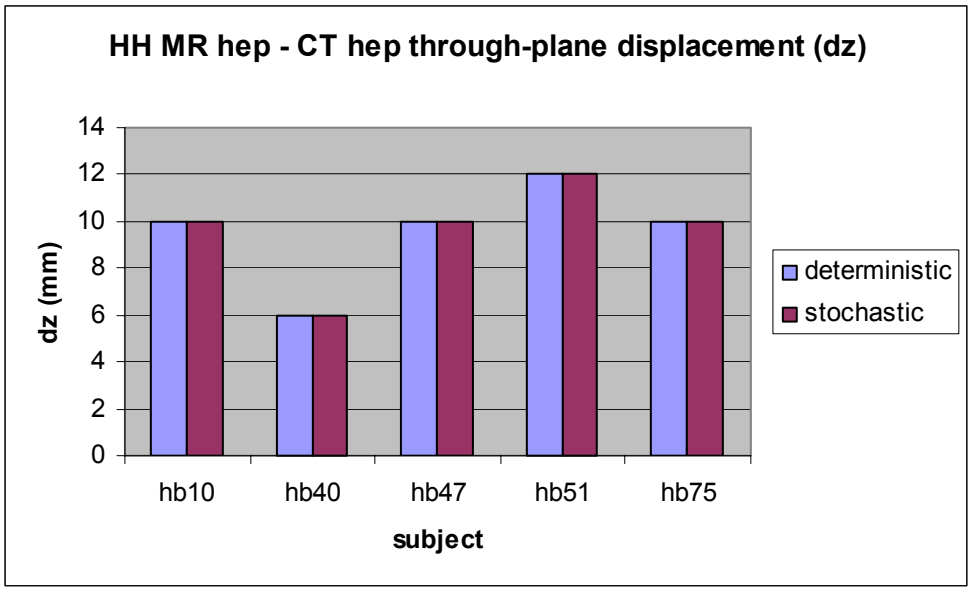

Figure 9b: Plot of through-plane displacement (dz) for sample MR-CT intermodality registration. Both the deterministic approach and the stochastic approach yielded the same through-plane displacement errors across subjects.

4.1.4 Visual Assessment Results

The mean displacement errors (both in-plane and through-plane) between the registered images were found using 20 automatically selected point landmarks. These control point pairs were chosen based on their image gradients. Simple visual inspection was performed to ensure that the points corresponded to the same anatomical feature in the two images. It was found that the control point pairs of the cases that were processed using the deterministic optimization scheme consistently demonstrated good correspondence whereas in contrast, the "multi-starts" approach often demonstrated poor correspondence.

4.2 ITK'S MULTIRESMIREGISTRATION SOFTWARE

4.2.1 Self-Validation Results

Similar to the self-validation tests performed on the head-and-hat surface fitting program, each image volume was registered using ITK's MultiResMIRegistration software to a second volume derived from the first with a known transformation. Out of the 162 CT image sets that were registered, 4 cases (2.5%) showed large divergence, whereas 2 cases (1.2%) showed slight divergence, all of which were subjected to a rotation in z plus translations in x, y, z. Out of the 720 MR image sets that were registered, 16 (2.2%) cases showed slight divergence, whereas 86 (11.9%) cases showed large divergence. The gradient descent optimizer used by the MultiResMIRegistration program seemed less prone to converging to the wrong optimum (i.e. diverging) than the optimizer based on Powell's method for the head-and-hat surface registration.

4.2.2 Intrasubject CT-CT Intramodality Registration Results

For intrasubject CT-CT intramodality registration, with the pre-contrast image as the target image and the contrast enhanced hepatic phase image as the moving image, the mean displacement between the control points was found to be 8.4mm. With the portal phase image as the moving image, the mean displacement was 7.7mm. Figures 10a and 10b are plots showing the breakdown of the displacement errors (in-plane and through plane) by subject. Displacement errors were slightly less for pre-contrast vs. portal phase cases.

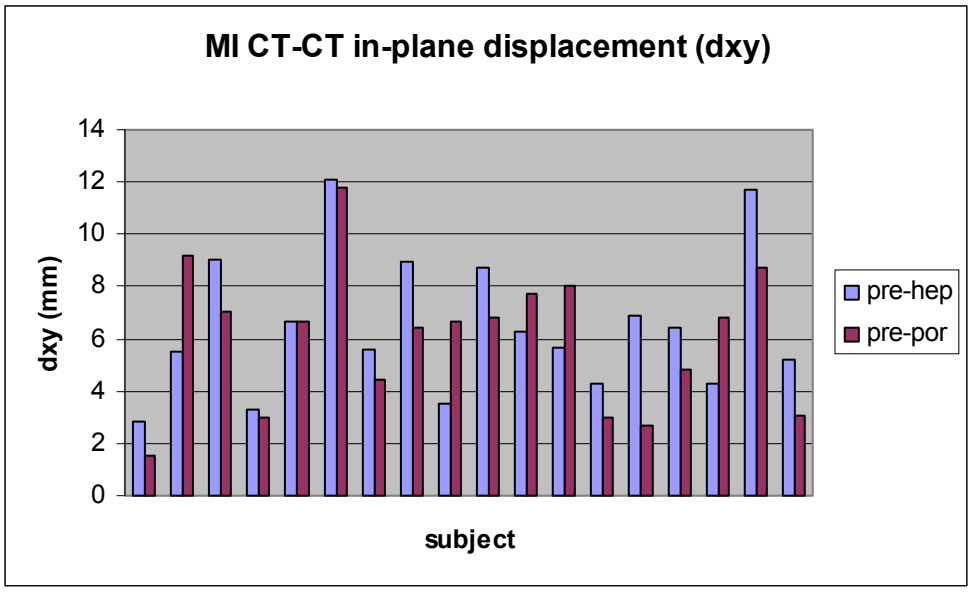

Figure 10a: Plot of in-plane displacement error (dxy) for two different combinations of intrasubject CT-CT intramodality registration (i.e. pre-contrast vs. hepatic phase & pre-contrast vs. portal phase). Note that the displacements were slightly less for pre-contrast vs. portal phase cases.

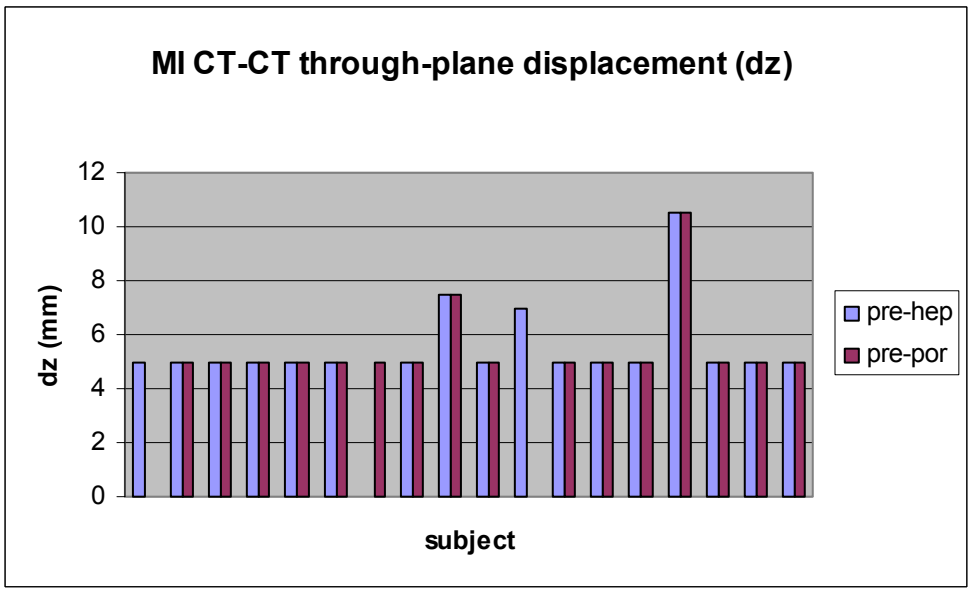

Figure 10b: Plot of through-plane displacement error (dz) for CT-CT intramodality registration. Note that zero placements are not plotted in the figure.

4.2.3 Intrasubject MR-MR Intramodality Registration and Intrasubject MR-CT Intermodality Registration Results

For MR-MR intramodality registration, with the contrast enhanced hepatic image as the target, the mean displacement between the landmarks was 8.2mm. Plots of the in-plane and through-plane displacement errors are shown in figures 11a and 11b. For MR-CT intermodality registration, with the contrast enhanced hepatic phase MR image as the target and the contrast enhanced hepatic phase CT image as the source, the mean displacement was 18.9mm. With the portal phase CT image as the source, the mean displacement was found to be 14.0mm. Finally, with the pre-contrast CT image as the source, the mean displacement was 17.0mm. A breakdown of the displacement errors are shown in figures 12a and 12b. As a general observation, MR-CT intermodality registration produced the greatest amount of misregistration overall.

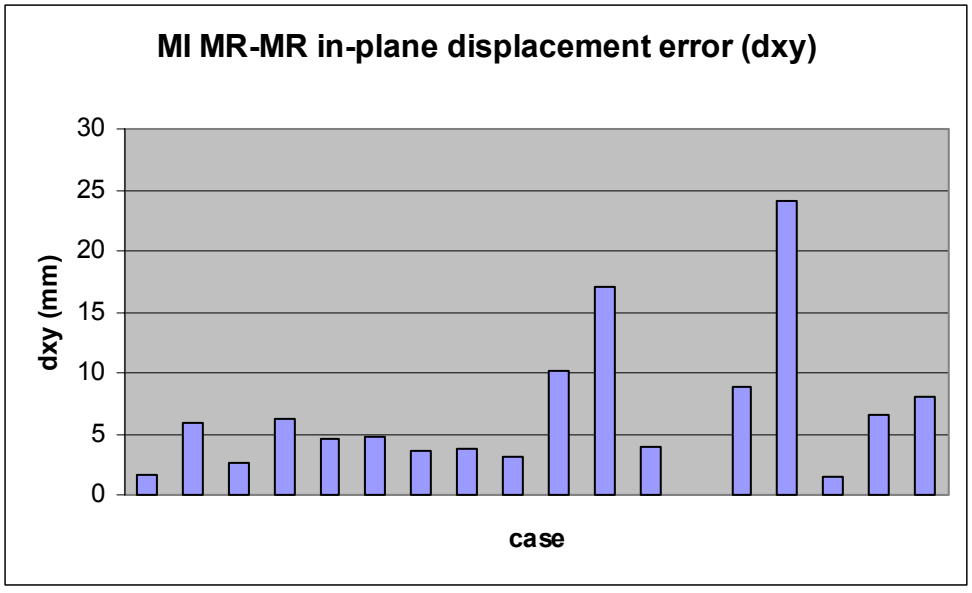

Figure 11a: Plot of in-plane displacement error (dxy) for intrasubject MR-MR intramodality registration by case.

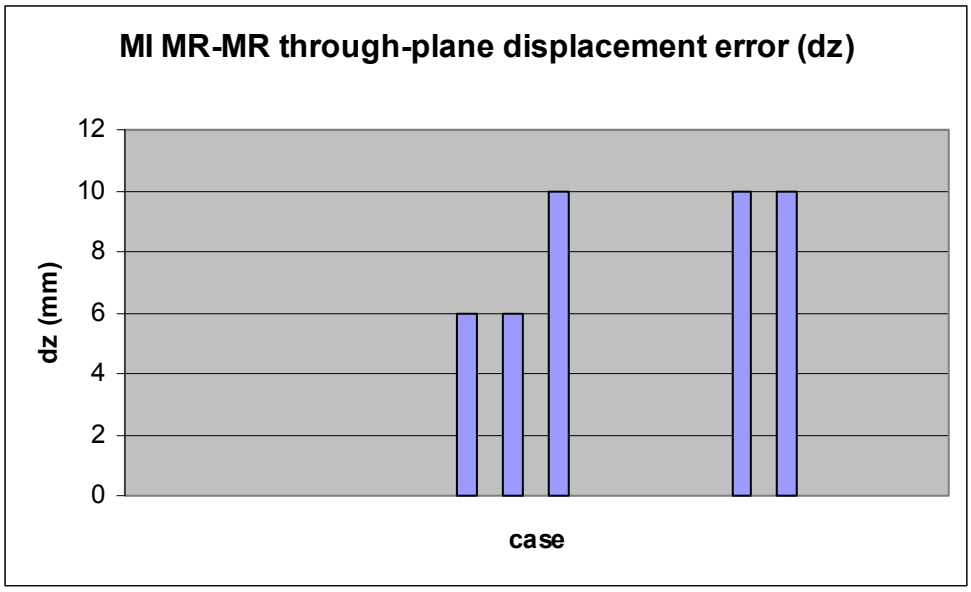

Figure 11b: Plot of through-plane displacement error (dz) of intrasubject MR-MR intramodality registration by case. Note that zero displacement errors are not plotted.

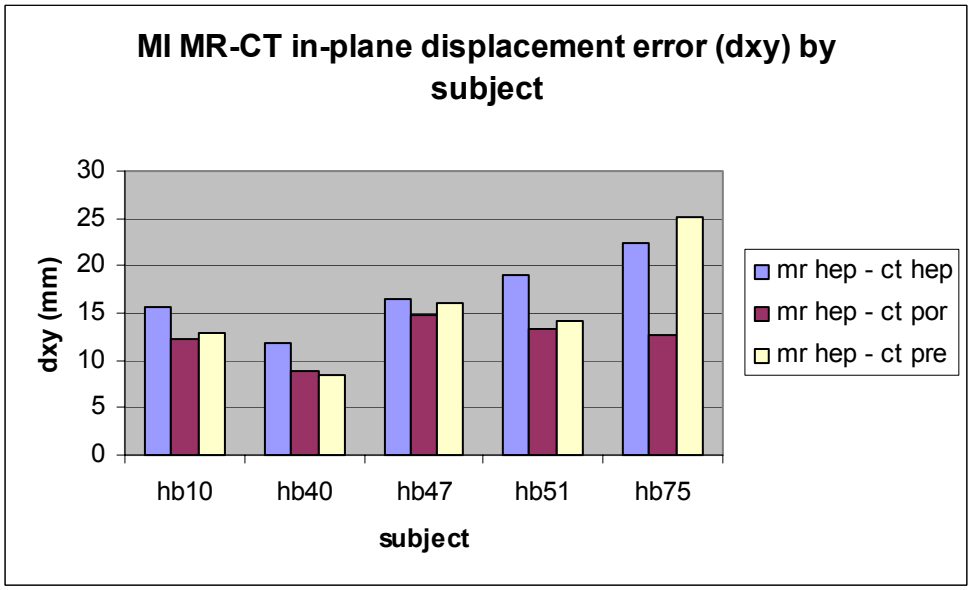

Figure 12a: Plot of in-plane displacement error (dxy) for intrasubject MR-CT intermodality registration (with the CT hepatic phase image, CT portal phase image, and CT pre-contrast image as the source).

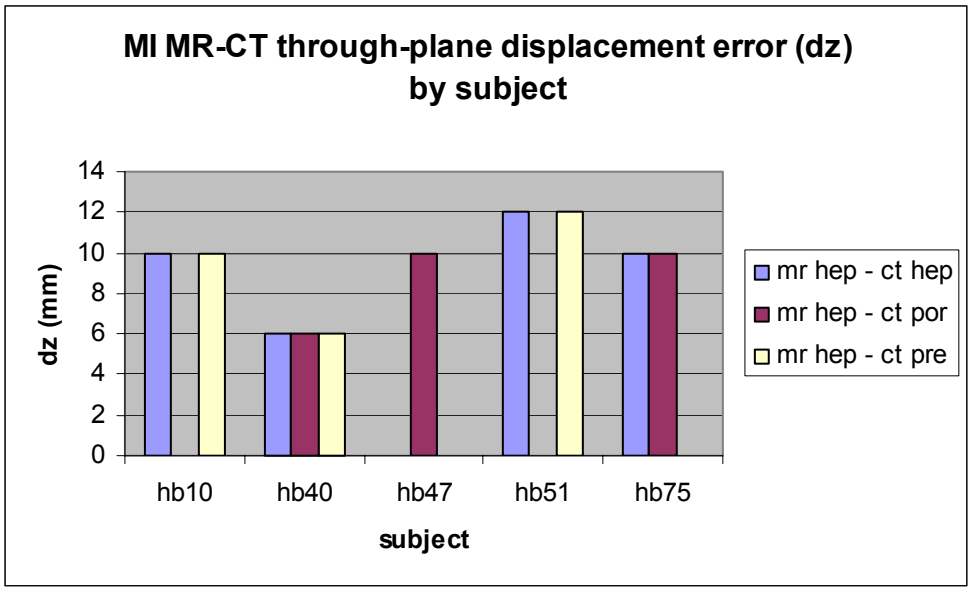

Figure 12b: Plot of through-plane displacement error (dz). Zero displacement errors are not plotted.

4.2.4 Visual Assessment Results

Similar to the head-and-hat surface registration technique, the amount of misregistration was quantified by measuring the displacements between automatically selected control point pairs. Visual inspection of the point pairs revealed that the majority of them corresponded to the same anatomical structure (or physical position in space) for different combinations of intramodality and intermodality registration.

4.3 HEAD AND HAT VS. MUTUAL INFORMATION REGISTRATION RESULTS

Here we report the results of a retrospective study on the efficacy of a surface-based (head-and-hat) scheme and a voxel similarity-based (mutual information) scheme in registering abdominal CT images without contrast, with contrast in the hepatic arterial phase, with contrast

in the portal venous phase, and contrast enhanced abdominal MR images. In particular, we report the amount of misregistration by subject, in-plane and through-plane displacement errors for intrasubject CT-CT intramodality registration (results are shown in figures 13a-c), intrasubject MR-MR intramodality registration (figures 14a-c), and intrasubject MR-CT intermodality registration (figures 15a-c) using a surface fitting strategy based on the technique proposed by Pelizzari et al. and voxel-based mutual information scheme distributed with the ITK Insight software package.

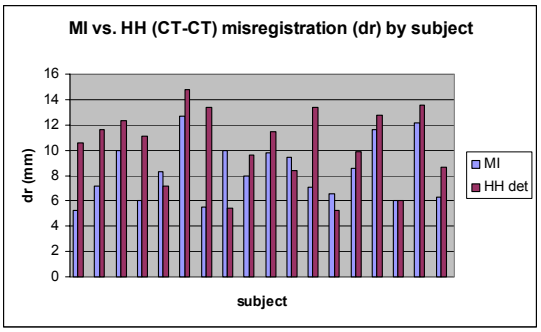

Figure 13a

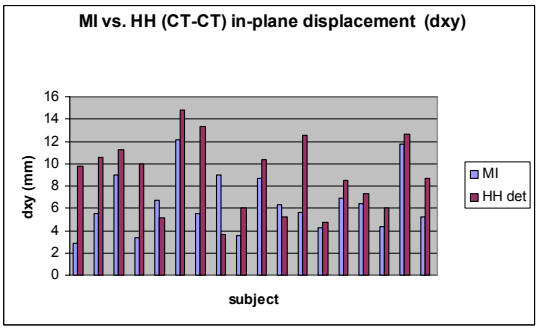

Figure 13b

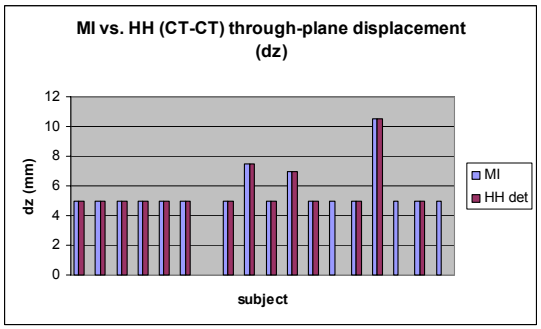

Figure 13c

Figures 13a-c: Plots of the amount of misregistration (top left), in-plane displacement error dxy (top right) and through-plane displacement error dz (bottom) for ***CT-CT intramodality registration based on the mutual information voxel similarity method (in blue) and the head-and-hat algorithm (red)***. Note the difference in performance of the two methods: the mutual information approach has consistently yielded smaller displacement errors than the surface-based approach.

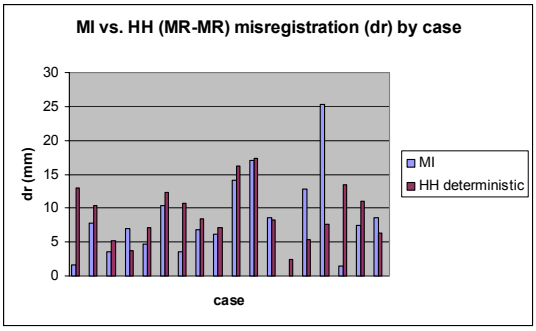

Figure 14a

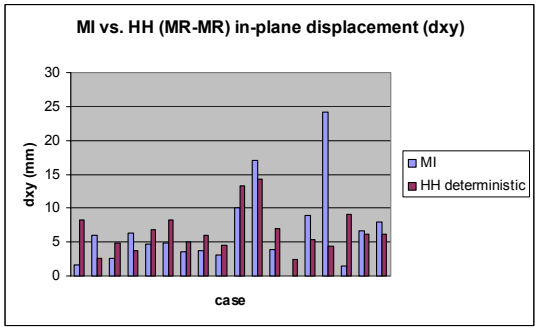

Figure 14b

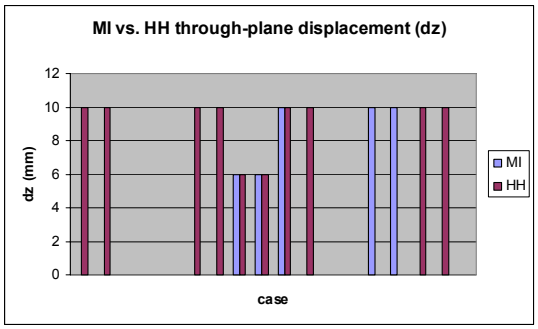

Figure 14c

Figures 14a-c: Plots of misregistration by subject (top left), in-plane displacement (top right) and through-plane displacement (bottom) for ***MR-MR intramodality registration based on the mutual information voxel similarity method (in blue) and the head-and-hat algorithm (red)***. Zero displacements are not plotted. Except for two cases, the two techniques produced similar results for registering intrasubject, intramodality MR images.

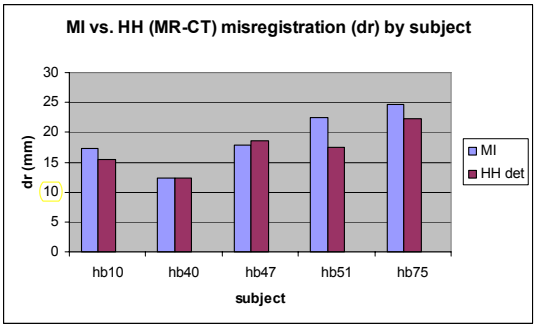

Figure 15a

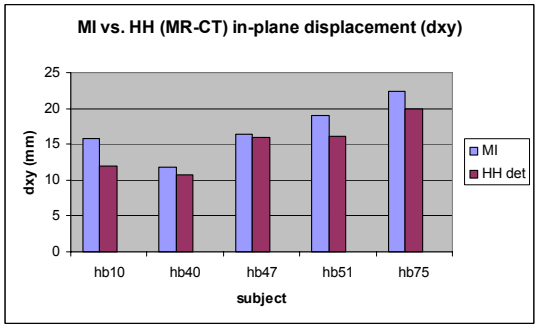

Figure 15b

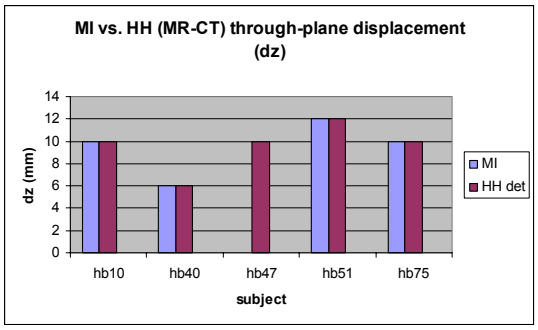

Figure 15c

Figures 15a-c: Plots of misregistration by subject, in-plane displacement and through-plane displacement (bottom) for ***MR-CT intermodality registration based on the mutual information voxel similarity method (in blue) and the head-and-hat algorithm (red)***. Similar displacement errors for the two techniques were observed.

The following figures are example images showing registration effect for CT-CT intramodality registration (figure 16), MR-MR intramodality registration (figure 17), and for MR-CT intermodality registration (figure 18).

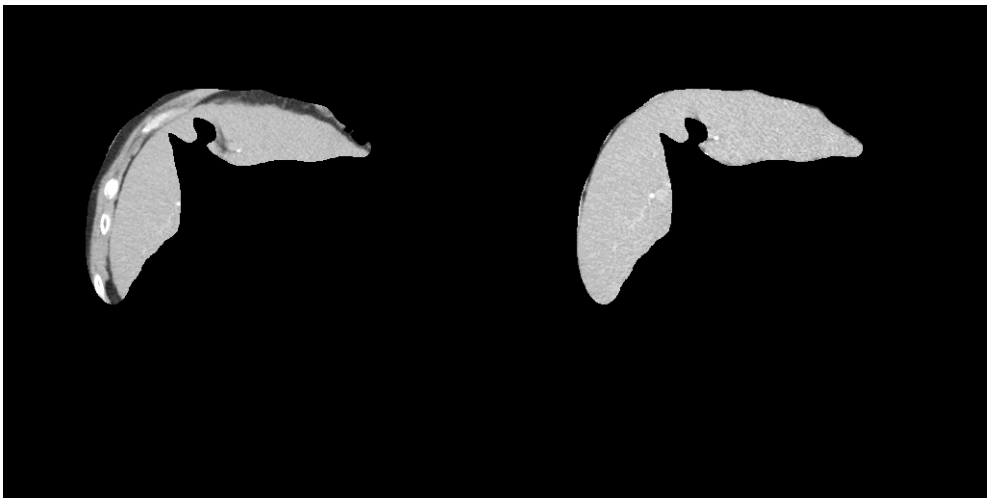

Figure 16: Example images showing registration effect for ***CT hepatic phase image registered to CT pre-contrast image***. On the left we have the registered source image (head-and-hat) multiplied by the target mask. On the right we have the registered source image (mutual information) source image multiplied by the target mask. Note the increased amount of non-hepatic structures within the masked region of the head-and-hat image (ribs).

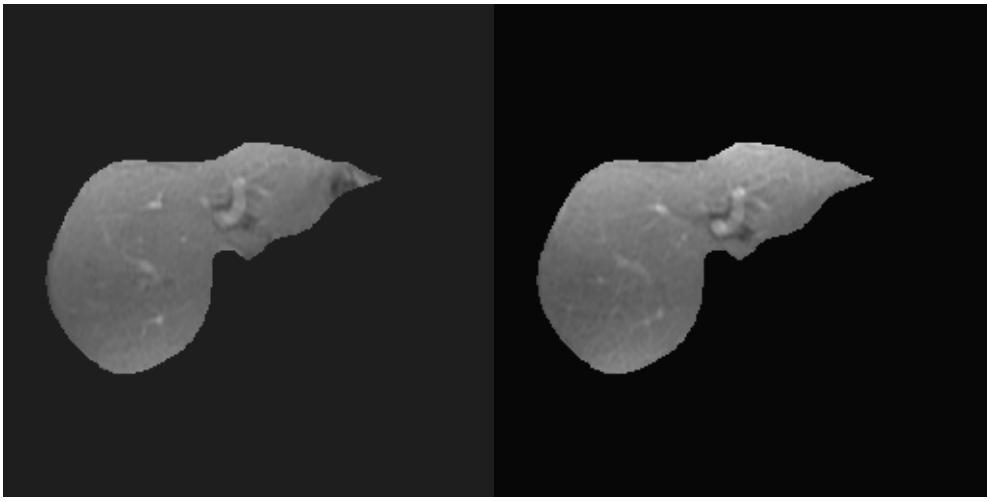

Figure 17: Example images showing registration effect for ***MR portal phase image registered to MR hepatic image***. On the left we have the registered source image (head-and-hat) multiplied by the target mask. On the right we have the registered source image (mutual information) source image multiplied by the target mask. Note the increased amount of non-hepatic structures within the masked region of the head-and-hat image (tip of the liver in the image on the left).

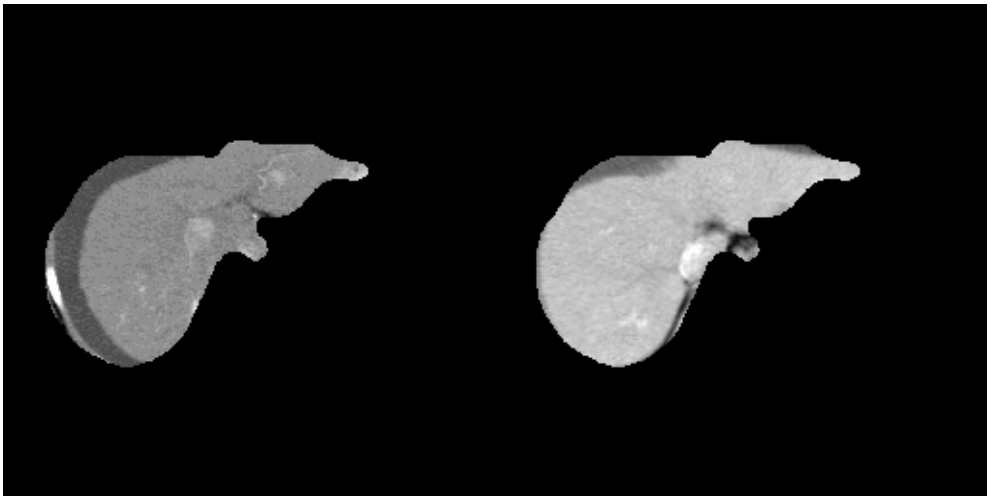

Figure 18: Example images showing registration effect for ***CT hepatic phase image registered to MR hepatic image***. On the left we have the registered source image (head-and-hat) multiplied by the target MR mask. On the right we have the registered source image (mutual information) source image multiplied by the target mask. Note the increased amount of non-hepatic structures within the masked region of the head-and-hat image (ribs).

Below are sets of pre- and post-registration images obtained using the mutual information voxel similarity registration framework. Figures 19a and 19b are two different intrasubject CT-CT intramodality registration cases (left image is the pre-registration image, whereas the post-registration image is on the right). Note the decreased amount of non-hepatic structures (ribs) within the masked region of the post-registration image (right).

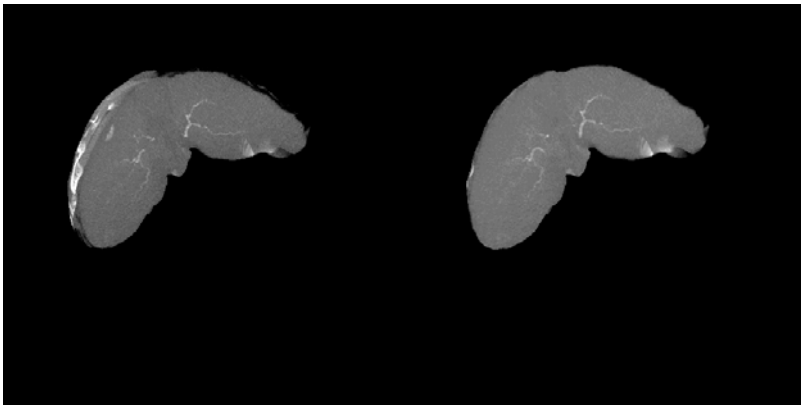

Figure 19a

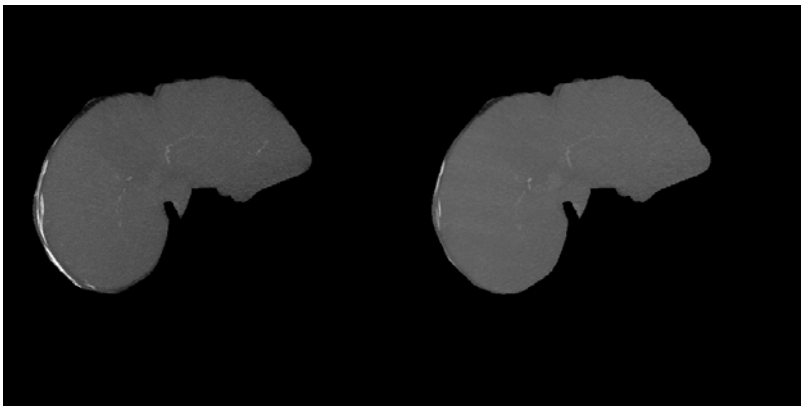

Figure 19b

Figure 19a-b: Pre- and post-registration images obtained using the mutual information voxel similarity registration framework. Note the decreased amount of non-hepatic structures (ribs) within the masked region of the post-registration image (right).

Figures 20a and 20b (shown below) are sets of pre- and post-registration images obtained using the head-and-hat surface registration scheme. The two figures represent two different

intrasubject CT-CT intramodality registration cases. Note that the amount of non-hepatic structures (ribs) within the masked region of the pre-registration image (left) is similar to the amount of the same non-hepatic structures within the masked region of the post-registration image (right).

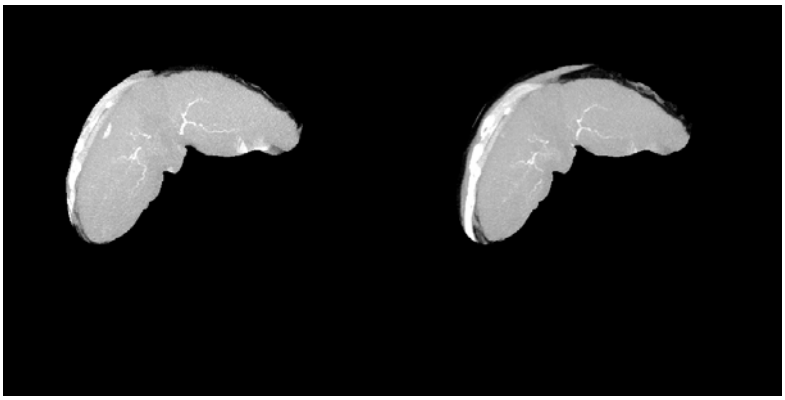

Figure 20a

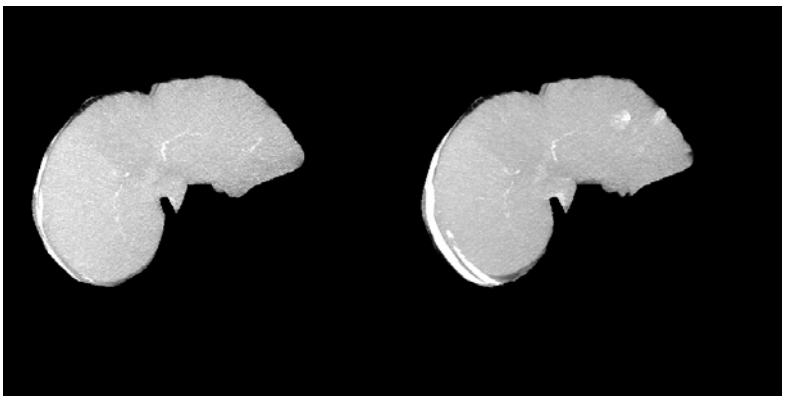

Figure 20b

Figure 20a-b: Pre- and post-registration images obtained using the head-and-hat surface registration scheme. Note that the amount of non-hepatic structures (ribs) within the masked region of the pre-registration image (left) is similar to the amount of the same non-hepatic structures within the masked region of the post-registration image (right).

5.0 DISCUSSION AND CONCLUSION

Image registration has been an area of active research and the state-of-the-art brain image registration solves many difficult clinical tasks. However, there is a relative shortage of image registration work outside the brain anatomy, and a dearth of literature on registration techniques devoted to registering images of the liver.

5.1 CHALLENGES WITH REGISTERING THE LIVER

Liver registration is challenging, the anatomy and inherent motion of the organ within the abdominal cavity with respiration place special constraints on the registration approach that can be used. The liver is essentially featureless and lacks visible surface landmarks on tomographic images, although a limited number of internal landmarks can be identified in MR images. Vessel branch points (for e.g. branch points between the inferior vena cava and the hepatic vein) are a good possibility, but they are hard to identify and difficult to centralize to a point.

As commonly applied to brain image registration, frame-based techniques or techniques that rely on the placement of external markers on the patient's body assume a rigid underlying anatomy and a fixed spatial relationship of this anatomy with respect to the outside markers. The liver can move significantly within the abdominal cavity, rendering such approaches inappropriate. These prospective techniques are obtrusive, and in general, have little clinical acceptability because they involve time-consuming acquisition protocols. Retrospective image registration, on the other hand, is non-obtrusive to the existing clinical practice and perhaps the only alternative in the case of abdominal organs.

5.2 REGISTRATION RESULTS

The superiority of a voxel-similarity-based over a surface-based approach for intramodality CT-CT registration, intramodality MR-MR registration, and intermodality MR-CT registration has been shown in this study. For the multi-resolution mutual information approach, mean misalignments were in the range of 7.7mm-8.4mm for CT-CT intramodality registration, 8.2mm for MR-MR intramodality registration, and 14.0mm-18.9mm for MR-CT intermodality registration. For the head and hat surface registration methods, mean misregistrations were in the range of 9.6mm-11.1mm for CT-CT intramodality registration, 9.2-12.4mm for MR-MR intramodality registration, and 15.2mm-19.0mm for MR-CT intermodality registration.

5.3 FACTORS RESPONSIBLE FOR MISREGISTRATION

5.3.1 Limitations of Surface-Based Registration Techniques

Retrospective registration approaches rely on anatomical point landmarks, contours or surface landmarks, or voxel similarity. Not many point landmarks can be reliably identified and used for liver registration. Contour or surface-based approaches rely on accurate segmentation of one or many anatomical structures in the images to be registered. As we have demonstrated in this study, segmentation of liver images is a difficult problem that usually requires manual intervention for optimal robustness and accuracy. If manual steps are involved, the accuracy of segmentation becomes user-dependent [22]. Segmentation-based registration is limited by the accuracy and reliability of segmentation (suffers from surface segmentation errors), lacks information about internal structures, and is restricted to a radial correspondence. Since we registered unmasked images of the liver to the masked image of the target volume when we

applied the voxel similarity-based registration technique, only segmentation of contours from the target image volume was required (thereby removing a significant amount of the extrinsic limits placed by manual segmentation on the registration accuracy). Therefore, the voxel-similarity-based approach appeared to be a better framework for liver registration.

5.3.2 Optimization Schemes

A requirement for successful registration is that the similarity function must be quasi-convex or well-behaved with as few local maxima/minima or ripples as possible [34]. This requirement has not been met in this study. Many of the cases that were registered using the head-and-hat method had large displacement errors because the optimizer failed to converge to the global minimum. A common stopping criterion for an optimizer is the maximum number of iterations allowed set by the user. It was suspected that for many of the cases that failed to converge, the optimization routine was terminated because the maximum number of iterations was met and not because the convergence criteria were satisfied.

Various manipulations in the registration procedure, such as interpolation and image subsampling, typically introduce local optima to the similarity function [17, 18]. The multi-resolution approach employed by ITK's mutual information scheme intended to improve computational efficiency could partially solve the problem of optimization in a search space of multiple optima.

5.3.3 Validation of Registration Accuracy

From the user's perspective, accuracy is one of the most important properties of a registration method. Validation of registration accuracy is generally not an easy task, because the

true answers (i.e. a set of gold standard answers that can serve as a basis for measuring accuracy) are usually not available. In the case of abdominal organs, registration accuracy is difficult to assess. As discussed earlier, many methods in the literature for brain registration are not applicable. Unlike the head, we cannot fix fiducial markers and obtain a gold standard, subvoxel measurement of the registration parameters. Instead, we are limited to anatomical landmarks. Due to the relative featurelessness of the liver and the small set of features identifiable across different CT phase images and MR images, we were forced to resort to using point landmarks selected based on image gradients. The automatic control point detection algorithm is a gradient-based approach where landmarks in the target image are identified from locations with strong gradients, matching locations in the source image are identified by examining the correlation between the gradient shape in a pre-defined search range of the target image landmarks. 20 point sets with the highest matching criteria were used to quantify the amount of misregistration. Unfortunately, errors can occur in the identification of the control point pairs and limit the ability of this validation approach to assess the registration accuracy.

5.3.4 Nature of Acquired Data

The data used in this study were acquired retrospectively, without steps taken prospectively to facilitate the evaluation of registration techniques. The images were not obtained in a controlled setting with triggering from respiratory bellows, intended to suppress inherent motion of the liver. The quality of the registration results was also limited by resolution (slice thickness) imposed by clinical constraints. Consequently, since the images had 10mm thick slices (MR) and 5mm thick slices (CT), we did not anticipate much lower displacements. For

almost all the cases examined, both registration techniques had a mean through-plane displacement equal to the slice thickness.

5.4 CONCLUSION

We have demonstrated that mutual information-based registration, originally applied to multimodality registration of brain images, is generally more effective than surface-based registration scheme for liver registration. Liver registration is extremely challenging because it lacks visible surface landmarks and that it moves within the abdomen with respiration. With these constraints, well-established registration techniques commonly used to register brain images, and validation methods based on point landmarks are not applicable. Our preliminary study assumed that the liver is a rigid body because the images used in our experiments were images of the stiff cirrhotic liver. Because the data was acquired retrospectively, without steps taken to facilitate the evaluation of registration techniques, and with rather thick slices of 5-10mm, mean displacements were 7.7-8.4mm (CT-CT), 8.2mm for intrasubject MR-MR intramodality registration, and 14.0-18.9mm for MR-CT intermodality registration for the multi-resolution mutual information registration scheme; and the mean displacements were 9.6-11.1mm (CT-CT), 9.2-12.4mm (MR-MR) and 15.2-19.0mm (MR-CT) for the head-and-hat surface fitting technique. Unlike registration for diagnosis and treatment in the brain, accuracy requirements are reduced for applications in the liver. Liver tumors are usually large, ranging in diameter from 1.2 to 18.8cm in clinical trials [7]. The liver is very resilient and often a tumor can be over-treated with little danger of serious complications. This is fortunate, since motion and deformation in the liver likely degrade the accuracy of rigid body registration (as we have seen in

this study). Prospective steps need to be taken to acquire images in a controlled setting to ensure the success of future studies in liver registration.

BIBLIOGRAPHY

[1] Audette, Michel A. et al. An Algorithmic Overview of Surface Registration Techniques for Medical Imaging. Medical Image Analysis 2000; 4(3): 201-217.

[2] Bankman, Isaac N. Handbook of Medical Imaging: Processing and Analysis. San Diego: Academic Press, 2002.

[3] Bookstein, FL. Morphometric Tools for Landmark Data. Cambridge: Cambridge University Press, 1991.

[4] Bunday, BD. Basic Optimization Methods. London: Edward Arnold Publishers Ltd., 1984.

[5] Capek, M et al.: Robust and fast medical registration of 3D-multi-modality data sets.

[6] Carrillo, Andres et al.: Semiautomatic 3-D image registration as applied to interventional MRI liver cancer treatment. IEEE Transactions on Medical Imaging 2000; 19:175-185.

[7] Christensen, GE et al.: Consistent image registration. IEEE Transactions on Medical Imaging 2001; 20:568:582.

[8] Dryden, IL et al. Statistical Shape Analysis. West Sussex: John Wiley & Sons,1998.

[9] Dugdale, PE et al.: Hepatic metastasis: the value of quantitative assessment of contrast enhancement on computed tomography. European Journal of Radiology 1999, 30:206-213.

[10] Duncan, James S. & Nicholas Ayache.: Medical Image Analysis: Progress over Two Decades and the Challenges Ahead. IEEE Transactions on Pattern Analysis and Machine Intelligence; 22(1):85-106.

[11] El-Serag, HB et al.: Rising incidence of hepatocellular carcinoma in the United States. The New England Journal of Medicine 1999; 340:745-750.

[12] Faber, TL et al. Spatial and temporal registration of cardiac SPECT and MR images: methods and evaluation. Radiology 1991; 179:857-861.

[13] Federle, MP et al.: CT evaluation of the liver: principles and techniques. Seminars in Liver Disease 2001; 21:135-145.

[14] Fitzpatrick, JM et al. Visual assessment of the accuracy of retrospective registration of MR and CT images of the brain. IEEE Transactions on Medical Imaging 1998; 17:571-585.

[15] Gao L. et al. Automatic liver segmentation technique or three-dimensional visualization of CT data. Radiology 1996: 201:359-364.

[16] Hawkes, DJ et al. Medical Image Registration. New York: CRC Press LLC, 2001.

[17] He, Renjie & Ponnada A. Narayana. Global optimization of mutual information: application to three-dimensional retrospective registration of magnetic resonance images. Computerized Medical Imaging ad Graphics 2002; 26:277-292.

[18] Herline, AJ et al.: Surface registration for use in interactive, image guided liver surgery. Computer Aided Surgery 2000; 5:11-17.

[19] Hill, DLG et al.: Medical image registration. Physics in Medicine and Biology 2001; 24:R1-R45.

[20] Kaneko T. et al. Abdominal organ recognition using 3D mathematical morphology. Proc. 15th International Conference on Pattern Recognition 2000; 2:263-266.

[21] Krinsky, GA et al.: MR imaging of cirrhotic nodules. Abdominal imaging 2000; 25:471-482.

[22] Hutton, Brian F. et al: Image Registration: An Essential Tool for Nuclear Medicine. European Journal of Nuclear Medicine 2002; 29(4): 559-577.

[23] Hutton, Brian F. & Michael Braun: Software for Image Registration: Algorithms, Accuracy, Efficacy. Seminars in Nuclear Medicine 2003; 13(3): 180-192.

[24] Levin, David N. et al.: Retrospective Geometric Correlation of MR, CT, and PET Images. Radiology 1988; 169:817-823.

[25] Lewin, JS et al. Interactive MRI-guided radiofrequency interstitial thermal ablation of abdominal tumors: Clinical trial for evaluation of safety and feasibility. JMRI 1998; 8(1):40-47.

[26] Lohmann, Gabriele. Volumetric Image Analysis. John Wiley & Sons Ltd: Chichester, 1998.

[27] Maes, F et al.: Multimodality image registration by maximization of mutual information. IEEE Transactions on Medical Imaging 1997; 16:187-198.

[28] Maintz, JBA et al.: A survey of medical image registration. Medical Image Analysis 1998; 2:1-36.

[29] Mathews, JH. Numerical Methods. Englewood Cliffs: Prentice-Hall, Inc., 1987.

[30] Murakami, T et al.: Imaging evaluation of the cirrhotic liver. Seminars in Liver Disease 2001; 21:213-224.

[31] Pelizzari, Charles A et al..: Accurate Three-Dimensional Registration of CT, PET, and/or MR Images of the Brain. Journal of Computer Assisted Tomography 1989; 13(1): 20-26.

[32] Press, WH et al. Numerical Recipes in C, 2nd Edition. Cambridge: Cambridge University Press, 1992.

[33] Robb, RA. Three-Dimensional Biomedical Imaging – Principles and Practice. New York: VCH Publishers, Inc., 1995.

[34] Rouet, Jean-Michel et al. Genetic Algorithms for a Robust 3-D MR-CT Registration. IEEE Transactions on Information Technology in Biomedicine 2000: 4(2): 126-136.

[35] Scott, AM et al. Clinical validation of SPECT and CT/MRI image registration in radiolabeled monoclonal antibody studies of colorectal carcinoma. Journal of Nuclear Medicine 1994; 35:1976-1984.

[36] Sethian JA. Fast marching methods. SIAM Review 1999; 41:199-235.

[37] Shekhar, Raj & Vladimir Zagrodsky. Mutual Information-Based Rigid and Nonrigid Registration of Ultrasound Volumes. IEEE Transactions on Medical Imaging 2002; 21(1): 9-22.

[38] Soler L. et al. Fully automatic, pathological, and functional segmentation from CT scans for hepatic surgery. Computer-Aided-Surgery 2001: 6:131-142.

[39] Thevenaz, P et al.: A pyramid approach to subpixel registration based on intensity. IEEE Transactions on Image Processing 1998; 7:27-41.

[40] Thurfjell, L et al.: Improved efficiency for MRI-SPET registration based on mutual information. European Journal of Nuclear Medicine 2000; 27:847-856.

[41] Udupa, JK et al. 3D Imaging in Medicine. Boca Raton: CRC Press LLC, 1991.

[42] West, J. et al.: Retrospective intermodality registration techniques for images of the head: Surface-based versus volume-based. IEEE Transactions on Medical Imaging 1999; 18:144-150

[43] Wang H, Zheng B, Good WF, Zhuang T. Thin-plate spline based automatic alignment of dynamic MR breast images. World Congress on Medical Physics and Biomedical Engineering, July 23-28, 2000.

[44] Wong, JCH et al. Evaluation of the limits of visual detection of image misregistration in a brain fluorine-18 fluorodeoxyglucose PET-MRI study. European Journal of Nuclear Medicine 1997; 24: 642-650.

[45] Woods, RP et al. MRI-PET registration with automated algorithm. Journal of Computer Assisted Tomography 1993; 17:536-546.